Master of Science Thesis

Comparison of LES techniques using a simplified model problem for non-premixed turbulent combustion

L.A.Klaessen

October 1, 2023

Aerodynamics

Faculty of Aerospace Engineering

TU Delft

Delft University of Technology

Comparison of LES techniques using a simplified model problem for non-premixed turbulent combustion

Master of Science Thesis

For obtaining the degree of Master of Science in Aerospace Engineering at Delft University of Technology

L.A.Klaessen

October 1, 2023

Faculty of Aerospace Engineering · Delft University of Technology

Delft University of Technology

DELFT UNIVERSITY OF TECHNOLOGY
DEPARTMENT OF AERODYNAMICS

The undersigned hereby certify that they have read and recommend to the Faculty of Aerospace Engineering for acceptance the thesis entitled **"Comparison of LES techniques using a simplified model problem for non-premixed turbulent combustion"** by **L.A.Klaessen** in fulfillment of the requirements for the degree of **Master of Science**.

Dated: October 1, 2023

Supervisors:

dr. S.J. Hulshoff

dr. M. Kotsonis

dr. I. Langella

Acknowledgements

12 years ago a journey started to obtain a double Masters Degree in Applied Physics and Aerospace Engineering. What started as an ambitious project, became a long-term project. I would like to express my sincere gratitude to my supervisor, dr. Steve Hulshoff for his continuous interest and support during this thesis. Without his advice, guidance and help, this thesis could not be completed.

Also I would like to express my gratitude to prof. dr. Dirk Roekaerts and dr. Michael Stöllinger and Gerasimos Sarras for their feed-back, advice and providing necessary data.
And last, but not least, my utmost gratitude goes to my parents, friends and wife Marinka. Without their support during desperate times, the double degree would not be finished.

Table of Contents

List of Figures

List of Tables

Chapter 1

Introduction

Currently there is a nitrogen crisis in the Netherlands and one of the consequences of this crisis is a delay in the permit application process which causes a (potential) delay of industrial projects related to the energy transition. To tackle this problem, solutions which reduces the emission of NO_x have to be found in a short time span.

One potential solution is an innovative combustion technology which is called Moderate or Intense Low-Oxygen Diluted (MILD) combustion, which is classified as a non-premixed combustion technology. In approximately the last three decades, MILD combustion has been extensively researched and developed to reduce the emission of greenhouse gasses in combustion applications. This technology is already used in the steel industry, but MILD combustion for a liquid fuel is not fully understood [51]. One of the characteristics of MILD combustion is a diluted oxidizer or fuel stream. Diluting the fuel or oxidizer stream results in slower chemical reactions, which lead to a larger reaction volume and this results in a more distributed energy release. The latter reduces the peak temperature and one of the consequences is a lower NO_x formation [30].

In the work of Klaessen [30], an attempt is made to perform a Large Eddy Simulation (LES) of MILD combustion to gain better insight into MILD combustion process. For this purpose, a filtered-based Large Eddy Simulation is used combined with several models to close unresolved terms in the filtered equations. Two of these models are the Eddy Viscosity model and the gradient assumption which respectively close the turbulent stress term and the turbulent scalar flux term. The use of a filtered-based LES and an Eddy Viscosity model is common for non-premixed combustion problems. A major drawback of these models is that they will always be non-zero when the gradient of the filtered quantity is non-zero. When the flow is captured in the resolved space, these subgrid terms should be zero. Also due to the application of a filter with non-uniform filter width, commutation errors are introduced. The reason for this is that a filter with non-uniform width does not commute with spatial derivatives.

In order to get better insight into MILD combustion, the methods used should be as efficient as possible to permit wide investigations of different flow conditions. One method to solve these

problems is to implement a more sophisticated LES model, for example the Variational Multiscale Method (VMM). This work will focus on the application of VMM to the modelling of non-premixed combustion.

1.1 Challenges in turbulent non-premixed combustion

One of the challenges in turbulent combustion is the large number of species and reactions involved in detailed kinetic mechanisms. For example, in the combustion process of methane and heptane, there are respectively 50 and 1000 species involved [32]. This number increases for larger hydrocarbons, such as diesel or kerosine. Methods have therefore been developed to reduce the number of species and chemical reactions. One of these methods is skeletal reduction [35]. The first level of reduction is the extraction of species and chemical reactions with little or no influence to the computations of the relevant chemical features. The second level of reduction is to identify fast chemical reactions or groups of fast reactions in partial equilibrium. This method identifies species which are in quasi steady state [13]. With skeletal reduction it is possible to reduce the number of species to the order of 15-40 species for simple hydrocarbons over a range of conditions [13, 50].

Another challenge in turbulent combustion is the large range of length and time scales. As stated above, many chemical reactions occur in combustion which lead to separated, discrete time scales due to different reaction rates [38]. The smallest time scale is of the order 10^{-10} s. The length scales can vary from those of the combustion apparatus down to the Kolmogorov length scales, and even smaller scales in the reaction zones. The existence of the large range of other scales imposes challenges into modelling turbulent combustion, because all the scales need to be computed and/or modelled, depending on the choice of modelling technique.

A final challenge in turbulent combustion is the coupling between molecular diffusion and chemical reaction. In turbulent combustion there exist two types of mixing: inert and reactive mixing. Inert mixing is the molecular mixing of conserved quantities such as inert species or mixture fraction, whereas reactive mixing is the molecular mixing of reactive species during chemical reactions. For inert mixing, the turbulent cascade tends to steepen gradients [52]. At high Reynolds numbers, the mean scalar dissipation scales with the inverse of the turbulent integral time scale [44] due to the rate-delimiting process of scale reduction through the turbulent cascade. Scaling with turbulent time scales shows that this process is independent of the molecular diffusivity. Therefore modelling inert mixing is not a major obstacle in turbulent combustion.

During reactive mixing however, chemical reactions occur. These can also steepen scalar gradients. The relative effectiveness of turbulent straining and chemical reaction in steepening scalar gradients depends on the chemical timescale, as well as the turbulent time scale of the smallest scales (the Kolmogorov time scale). The ratio of the Kolmogorov and chemical timescale is defined as the Karlovitz number, Ka. For sufficient large Ka, chemical reactions influence scalar gradients, therefore mixing is dominated by chemical reactions and diffusion. This corresponds to flamelet combustion, which occurs in a very thin layer where locally one-dimensional flamelet structures are present within the turbulent flow field.

1.2 A brief description of a selection of sophisticated LES models

One sophisticated modelling approach is implicit LES (ILES). Typically ILES uses filters to separate the scales, but no subgrid-scale model is added to the governing equations. Instead, the numerical numerical truncation error derived by considering the modified equation acts as the subgrid-scale model [1]. However, the ILES method should be applied with great caution. In real problems, the prediction of the dissipative properties of the numerical method is exceptionally difficult [11]. For the application of ILES to combustion, relatively little research has been conducted. For high-speed premixed flows, numerical simulations with acceptable results have been performed [28, 29, 55]. This work has been extended to low-speed premixed turbulent combustion by Zhao [54] and applied on a 1D laminar premixed flame.

A derived approach from ILES is the Variational Multiscale Method (VMM). Instead of filters, variational projections are used to express the large scales in appropriate spaces. Another feature of this method is a focus on modelling the fine-scales equations while maintaining the numerical consistency of the coarse scales equations. This permits full rate-of-convergences of the imposed numerical method, which is not necessarily the case with the traditional approach. Hughes [22] started the development of the VMM method, which is in principle a stabilizing method. The first versions of the VMM model for LES [24, 25] divided the scales into two separate scales: the coarse scale and fine scale. Often these scales are also referred as the resolved scales and unresolved scales respectively. Inspired by the traditional models, initially the artificial eddy-viscosity model was used. Initially this was included on the fine scale equations and acted on the fine scales only. In the work of Collis [10] and Gravemeier [15], this approach was clarified by dividing the scales into large coarse scales, small coarse scales and fine-scales. In this case the fine-scales are dependent on the small coarse scales only. With this technique Gravemeier [16] modeled the fine-scales with the Smagorinsky model.

Another method to approximate the fine-scales is based on the residual of the governing equation. When it's assumed that the non-linear fine-scales are small compared to the coarse scales, the leading term after linearization is explicitly dependent on the resolved scale residual [47]. Calo [6] exploited this idea by presenting the fine-scales as a function of the residual and the local Greens function. When applying the residual-based technique, VMM shuts off in a laminar flow because the fine-scale velocity is in this case equal to zero, whereas an eddy-viscosity model in traditional LES limits the rate of convergence because it is applied on all coarse scales. When the local Greens function is approximated by an element-averaged Greens function, the formulation resembles stabilization method [6, 21]. Stabilized methods add a weighted residual to the Galerkin formulation multiplied by the parameter τ [18]. For numerous equations stabilized methods have been developed, for example the (compressible)Euler and Navier-Stokes equation [48], the convection-diffusion equation [23] and the convection-diffusion-reaction equation [19, 7]. Bazilevs et al. [2] applied the residual-based methodology with the use of a stabilization parameter for incompressible homogeneous isotropic turbulence and turbulent channel flows. The presented cases use the quasi-static subscales assumption, which means that the fine-scales are independent of time. [9] presented a formulation which allows a time-dependent fine-scale approximation for incompressible flow problems. One of the main conclusions is that for a transient incompressible flow problem there are a lot of benefits to track the subscales in time including the application of time-independent stabilized parameters, which are extensively researched.

In literature, references considering VMM in combination with combustion are limited. Gravemeier and Wall [17] made an attempt to use VMM for the numerical case of a flame-vortex interaction, an example of premixed combustion. In this work, the two-scale residual based VMM with a stabilized method and with a Smagorinsky model for the fine-scales which is only dependent on the small coarse scales are implemented and compared to each other.

1.3 Objective of the thesis

There is a need to examine the potential of alternative methods such as VMM for the ability to improve the efficiency of combustion simulations. However the computational expense of a LES run of a 3D turbulent non-premixed combustion problem is high due to the large variety of length and time scales in turbulent non-premixed combustion. Secondly, VMM is a sophisticated model and the models used to simulate turbulent non-premixed combustion are complex. This means that the implementation of VMM in a turbulent non-premixed combustion increases the complexity even more. And finally, the results of a full 3D turbulent non-premixed combustion simulation are difficult to interpret due to their complexity.

Therefore the objectives of this thesis are as follows: Firstly to define a simplified model problem which has the important aspects of turbulent non-premixed combustion for comparing numerical methods. One goal of this objective is to reduce the complexity of the problem but include the important characteristics in order to minimize the possibility of cancelling errors and to minimize ambiguities in the results. Secondly, to propose and to investigate the potential of a framework based on VMM formulation for non-premixed combustion computations. The results of the simplified model problem in a VMM framework are compared to the results when using a standard Smagorinsky model. The simplified model problem focuses on the determination of velocity and mixing of scalars, a key concept of non-premixed combustion problems.

The objectives lead to the following research questions:

RQ1 What are the differences between the simplified model and a full 3D non-premixed combustion model?

RQ2 Are the current formulations of VMM sufficient for the simplified model problem?

RQ3 How do the methods compare in their ability to reproduce the statistics of the relevant variables?

RQ4 Which of the τ definitions for the flow field, reaction terms and for a passive scalar are most effective?

RQ5 What is the performance of the different assumptions for the subscales on the results?

1.4 Outline of the thesis

The thesis is organized as follows. Chapter 2 provides a description of the simplified model problem. The choices of the simplifications are explained and the governing equations are presented in this chapter. Chapter 3 provides the theoretical background information about the Variational Multiscale Method (VMM) and the implementation of LES in a VMM environment. The relevant coarse scales and fine-scales equations are derived, which is implemented in the LES code. In chapter 4 the test cases of the Method of Manufactured Solutions are explained and the results are presented. The SMP reference results and the results of the comparison of the different models are respectively shown in chapter 5 and 6. Finally, chapter 7 contains the conclusions and recommendations for future work.

Chapter 2

Simplified model problem and governing equations

The objective of this chapter is to introduce a simplified problem which models the important characteristics of non-premixed combustion. In the first section, the requirements and construction of the simplified model problem are presented. The second section shows the governing equations of the simplified model problem are derived. Because the simplified model problem should replicate the important characteristics of non-premixed combustion, one of the governing equation includes a non-linear source term.

2.1 A brief description of modelling non-premixed combustion

Non-premixed combustion is characterized by the presence of a non-premixed (or diffusion) flame. In such a flame, fuel and oxidizer are present in a separate stream. Fuel and oxidizer come together due to molecular diffusion and mix in a thin layer such that a combustible mixture is created. If ignition occurs, the combustible mixture ignites and heat is released. Far away from the thin layer, or reaction layer, the mixture is either too lean or too rich so that ignition is not possible (see Fig. 2.1). In the specific case that a flame front is very thin compared to other flow and wrinkling scales, the gradients along the flame front can be neglected comparing to the gradient normal to the flame front. This implies that the flame structure is locally 1D. When irreversible, infinitely fast chemistry is assumed, the flame structure depends only on time and mixture fraction. Such a small element of the flame front which shows 1D behavior is called a flamelet and therefore this assumption is called the flamelet assumption. The mixture fraction tracks the mixing of fuel and oxidizer in the flow. By definition, the mixture fraction is 1 in the fuel stream and 0 in the oxidizer stream. In Figure 2.2, an example is shown for the mixture fraction distribution of a jet flow. There are several methodologies available to solve a non-premixed combustion problem. In the work of Klaessen [30], the following decomposition into two subproblems is used, namely:

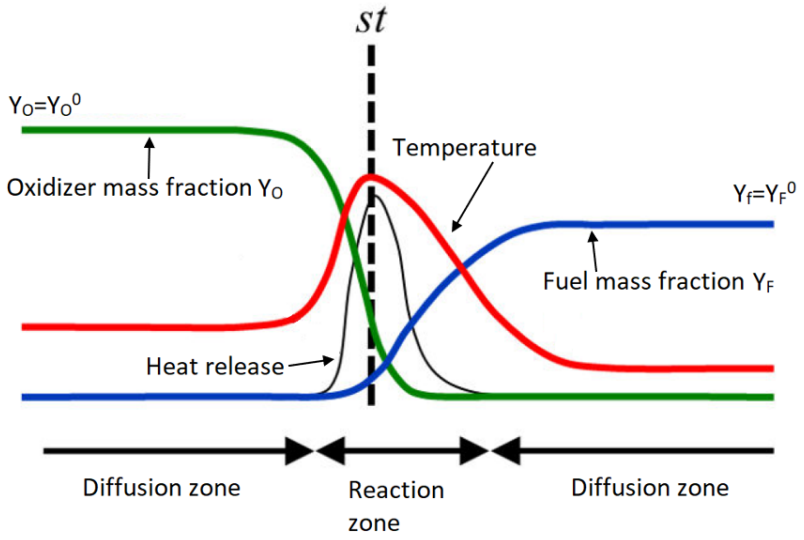

Figure 2.1: Structure of a non-premixed (or diffusion) flame. Superscript 0 denotes the mass fraction originating from the stream.

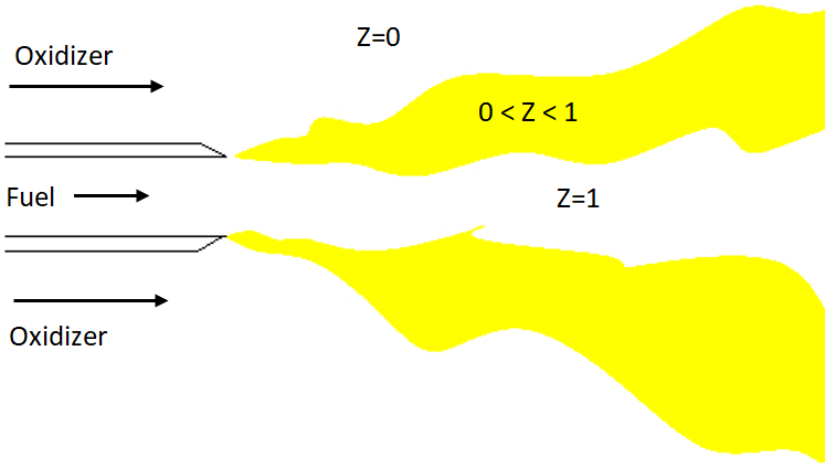

Figure 2.2: Representation of the mixture fraction in a jet flow

1. A mixing problem. In this problem the flow properties (velocity) and predefined scalars are calculated. These variables are input for the next subproblem;

2. A flame structure problem. In this problem the output of the mixing problem is processed in order to retrieve the thermochemical variables, such as temperature or chemical source term.

Some variables, such as viscosity, are dependent on temperature. Therefore solving the mixing problem and flame structure problem is an iterative process.

Imposing the assumptions of irreversible, infinitely fast chemistry and steady flamelets the flame

structure problem leads to a description which is only dependent of the mixture fraction Z and therefore contains no information about chemical reactions and cannot account for chemical variations in directions perpendicular to its gradient [39]. As a result flame lift-off and other ignition and extinction phenomena cannot be predicted accurately [40]. One solution for this problem is to apply the flamelet/progress variable approach, developed by Pierce and Moin [39]. The idea of the approach is to introduce another tracking scalar which is independent of the mixture fraction. This means that the new scalar must be a nonconserved scalar, in this case the reaction progress variable ϕ. The progress variable measures the extent-of-reaction of the flow. For example, the progress variable could be defined as a normalized summation of the mass fractions of reaction products. By definition, the progress variable is equal to 0 in fresh gasses and 1 in fully-burnt gasses. The application of the flamelet/progress variable approach results in a flame structure problem in which thermochemical variables are dependent on Z and ϕ.

A detailed description of the theory of non-premixed combustion can be found in Appendix A.

2.2 Requirements and construction of the simplified model problem

In more detail, the approach used for the DJHC-simulations of Klaessen [30] can be summarized in the following three steps:

1. Determine the 3D velocity field by solving the incompressible Navier-Stokes equations
2. Determine the mixture fraction Z and the progress variable ϕ in 3D
3. Determine the thermochemical variables, such as the chemical source term. These variables are based on the mixture fraction and the progress variable.

Thus solving a turbulent non-premixed problem is expensive, primarily due to step 1, but also step 2 and step 3. Testing a new model or discretisation technique for such a problem would be a cumbersome process. The run time of one calculation is in the order of weeks and testing a new model or new discretisation technique requires many runs. Therefore, a simplified model problem which has the important characteristics of turbulent non-premixed combustion is needed to facilitate rapid comparisons in order to determine its performance.

In Section 2.1, it is shown that a non-premixed combustion problem can be decomposed into a mixing problem (step 1 and 2 of the solution algorithm) and a flame structure problem (step 3 of the solution algorithm). To reduce complexity, the simplified model problem should only focus on one of these problems. The choice is based on the second objective of this thesis, which is to introduce the simplified model problem in a VMM framework. Because the VMM framework is an alternative to filtered Large Eddy Simulation, the most relevant differences will occur in the mixing problem, affecting the velocity field, mixture fraction and progress variable. Thus the flame structure determination is discarded from the simplified model problem and replaced by an analytical function.

A further simplification is to reduce the number of dimensions from three to one. This aids interpretation and increases efficiency, but must be done in a way which retains the important characteristics of the original problem. The approach used here is elaborated in the following section.

2.3 Simplification of the mixing problem

The mixing problem in [30] uses the 3D incompressible Navier-Stokes equations to compute the velocity field, the 3D convection-diffusion (CD) equation to compute the mixture fraction Z and the convection-diffusion-reaction (CDR) equation to determine the progress variable ϕ. The incompressible formulation is used because the relevant density variations are not caused by compressibility effects, but due to temperature variations and due to mixing of species with a different density.

The resulting system of the Navier-Stokes equations Eq.(A.11), the CD equation Eq.(A.50) and the CDR equation Eq.(A.57) can be written as:

$$\rho\frac{Du_j}{Dt} = -\frac{\partial p}{\partial x_j} + \frac{\partial}{\partial x_j}\left(\mu\left(\frac{\partial u_i}{\partial x_j} + \frac{\partial u_j}{\partial x_i} - \frac{2}{3}\frac{\partial u_i}{\partial x_i}\right)\right) \tag{2.1a}$$

$$\rho\frac{DZ}{Dt} = \frac{\partial}{\partial x_i}\left(\rho D_Z\frac{\partial Z}{\partial x_i}\right) \tag{2.1b}$$

$$\rho\frac{D\phi}{Dt} = \frac{\partial}{\partial x_i}\left(\rho D_\phi\frac{\partial \phi}{\partial x_i}\right) + \rho\dot{\omega}_\phi \tag{2.1c}$$

where u_i is the velocity in direction i, p is the pressure, ν is the kinematic viscosity, D_Z and D_ϕ are the diffusivity for the CD and CDR equation, respectively. The chemical reaction term in the CDR equation is denoted as $\dot{\omega}$.

In order to simplify the mixing problem Eq.(2.1), all terms are expanded and rearranged such that terms which are dependent on x and t are on the left-hand side and the remaining terms are on the right-hand side. After expanding and rearranging Equation (2.1a) in x-direction and assuming ρ and μ is constant, the result is:

$$\frac{\partial u}{\partial t}+u\frac{\partial u}{\partial x}-\nu\frac{\partial^2 u}{\partial x^2} = -\frac{1}{\rho}\frac{\partial p}{\partial x}-v\frac{\partial u}{\partial y}-w\frac{\partial u}{\partial z}+\nu\left(\frac{\partial^2 u}{\partial y^2}+\frac{\partial^2 u}{\partial z^2}\right)-\frac{1}{\rho}\frac{\partial}{\partial x}\left(\mu\frac{2}{3}\left(\frac{\partial u}{\partial x}+\frac{\partial v}{\partial y}+\frac{\partial w}{\partial z}\right)\right) \tag{2.2}$$

where $\nu = \frac{\mu}{\rho}$.

After expanding and rearranging Eq.(2.1b) and Eq.(2.1c) and assuming ρ, D_Z and D_ϕ is constant, the result is:

$$\frac{\partial Z}{\partial t} + u\frac{\partial Z}{\partial x} - D_Z\frac{\partial^2 Z}{\partial x^2} = -v\frac{\partial Z}{\partial y} - w\frac{\partial Z}{\partial z} + D_Z\left(\frac{\partial^2 Z}{\partial y^2}+\frac{\partial^2 Z}{\partial z^2}\right) + \frac{1}{\rho}\left(\frac{\partial \rho D_Z}{\partial x}\right) \tag{2.3}$$

$$\frac{\partial \phi}{\partial t} + u\frac{\partial \phi}{\partial x} - D_\phi \frac{\partial^2 \phi}{\partial x^2} - \dot{\omega} = -v\frac{\partial \phi}{\partial y} - w\frac{\partial \phi}{\partial z} + D_\phi \left(\frac{\partial^2 \phi}{\partial y^2} + \frac{\partial^2 \phi}{\partial z^2}\right) \tag{2.4}$$

It can be seen that the left-hand side is equal to the Burgers equation. The right-hand forcing term can be extracted from a 3D Navier-Stokes simulation. Eq.(2.3) and Eq.(2.4) are rearranged as such that the left-hand side is equal to respectively the 1D CD and the 1D CDR equation. If the right-hand side is also treated as a forcing term, both equations are simplified to its 1D counterpart including a forcing term. In summary, the forcing terms of the simplified version of the mixing problem are in this case defined as :

$$f_u = -\frac{1}{\rho}\frac{\partial p}{\partial x} - v\frac{\partial u}{\partial y} - w\frac{\partial u}{\partial z} + \nu\left(\frac{\partial^2 u}{\partial y^2} + \frac{\partial^2 u}{\partial z^2}\right) - \frac{1}{\rho}\frac{\partial}{\partial x}\left(\mu\frac{2}{3}\left(\frac{\partial u}{\partial x} + \frac{\partial v}{\partial y} + \frac{\partial w}{\partial z}\right)\right) \tag{2.5a}$$

$$f_Z = -v\frac{\partial Z}{\partial y} - w\frac{\partial Z}{\partial z} + D_Z\left(\frac{\partial^2 Z}{\partial y^2} + \frac{\partial^2 Z}{\partial z^2}\right) + \frac{1}{\rho}\left(\frac{\partial \rho D_Z}{\partial x}\right) \tag{2.5b}$$

$$f_\phi = -v\frac{\partial \phi}{\partial y} - w\frac{\partial \phi}{\partial z} + D_\phi\left(\frac{\partial^2 \phi}{\partial y^2} + \frac{\partial^2 \phi}{\partial z^2}\right) \tag{2.5c}$$

From Eq.(2.5), it can be seen that the forcing terms in the CD and CDR equation are a function of derivatives in the y and z direction. The forcing term in the 1D Burgers equation consists of a pressure term and derivatives in the y and z direction. In the next section, a detailed description is given of the behaviour of these simplified equations.

2.4 Characteristics of the simplified model problem

The following section briefly describes the governing equations of the simplified model problem. Three types of equations are used in this thesis, namely the Burgers equation for solving the velocity field, the convection-diffusion (CD) equation for solving the mixture fraction Z and the convection-diffusion-reaction (CDR) equation for solving the progress variable ϕ. In the following subsections, these equations are briefly explained.

2.4.1 Burgers equation

Eq. (2.2) is an example of the forced Burgers equation.

$$u_t + uu_i = \nu u_{ii} + f(x,t) \tag{2.6}$$

where u the velocity in x-direction, ν is the kinematic viscosity and the subscript t, i and ii denotes the derivative of the velocity in time, space and the second derivative in space respectively. $f(x,t)$ denotes the forcing term which accounts for the 3D-turbulent effects.

The Burgers equation was introduced in 1948 by J.M Burgers [4] as a simplification of the Navier-Stokes equation (in his paper referred as hydrodynamical equations) in an attempt to create a simplified system of mathematical equations used for studying the behaviour of turbulent motion. The strength of the Burgers equation is is that it can be solved analytically using Hopf-Cole transformation [20].

Because of their similarity, the Burgers and Navier-Stokes equations share some properties. For example, both equations show a forward energy cascade caused by the non-linear term and regions where high gradients occur are considered to be as regions with dissipation [34]. However, it must be understood that the Burgers equation lacks properties essential for modelling Navier-Stokes turbulence, namely the sensitivity to small perturbations in the initial conditions and therefore the spontaneous rise of instabilities resulting in turbulent eddies. Also the 3D vortex stretching mechanism is absent [43], although its effect on u is represented in f.

2.4.2 Convection-diffusion equation

The convection-diffusion (CD) equation Eq. (2.3) describes the physical phenomena where a physical quantity, such as particles or energy, are only transported in a domain due to convection and diffusion. In the simplified model problem the CD-equation is used for the determination of the fuel to oxidiser ratio or mixture fraction Z and it has a one-way coupling to the velocity field, which means that velocity alters the transport of the mixture fraction but there is no coupling to the flow field. This means that the mixture fraction has no influence on the flow fluid, thus no effect on density, viscosity and other flow variables.

For the simplified model problem, the CD equation has the following form:

$$Z_t + uZ_i = D_z Z_{ii} + g(x,t) \tag{2.7}$$

where Z is the mixture fraction, u the velocity in x-direction, D_Z is the diffusive coefficient or Z t, i and ii denotes the derivative in time, space and the second derivative in space respectively and $g(x,t)$ is a forcing term which accounts for the 3D-turbulent effects.

2.4.3 Convection-diffusion-reaction equation

The incompressible convection-diffusion-reaction (CDR) equation Eq. (2.4) describes the physical phenomena where a physical quantity, such as particles or energy, are transported in a domain due to convection, diffusion and reaction. In the context of this thesis, the CDR equation describes how the mass fraction of the reaction products or progress variable is distributed in a medium under the influence of convection, diffusion and chemical reactions.

For the simplified model problem, the CDR equation has the following form:

$$\phi_t + u\phi_i = D_\phi \phi_{ii} + \dot{\omega} + h(x,t) \tag{2.8}$$

where ϕ is the progress variable, D_ϕ is the diffusive coefficient of ϕ, $\dot{\omega}$ is the chemical reaction term and $h(x,t)$ is a forcing term. In this thesis the forcing term is chosen as such that it accounts for the 3D-turbulent effects. A model for $\dot{\omega}$ must be applied to solve the CDR equation. As stated in Section 2.3, for the simplified model problem an analytical function shall be used. In the next section, the derivation of this analytical function is shown.

2.5 Chemical reaction term modelling

The evaluation of chemical reaction terms remains a challenge due to their highly non-linear character. Usually they are based on a detailed or a reduced chemical mechanism, which requires complicated models in order to produce accurate results.

In some studies, e.g. in the work of Hauke and Garcia-Olivares [19], this term is simplified by using a linear function of ϕ to reduce the complexity and thus decreasing the run time. In this section a more general simplification of the chemical reaction term is derived based on a third order polynomial of ϕ.

Thermodynamic data from a chemical reaction scheme can be obtained from experiments, academic data sets or from specialized software. Here the chemical reaction term data of the work from Klaessen [30] is used for the polynomial fit routine.

We assume chemical source term $\dot{\omega}$ of the following form:

$$\dot{\omega} = A_0(x,t) + A_1(x,t)\phi + A_2(x,t)\phi^2 + A_3(x,t)\phi^3 \tag{2.9}$$

The global coefficients A_0, A_1, A_2 and A_3 are a function of space and time. A polynomial fit has to be constructed for these global coefficients. Due to the limits of the polynomial fit routine, a fifth order function for these global coefficients is constructed. Eq.(2.9) now becomes:

$$\begin{aligned}\dot{\omega} = &\left(a_0 + b_0 t + c_0 x\right)^5 + \left(b_1 + c_1 t + d_1 x\right)^5 \phi \\ &+ \left(b_2 + c_2 t + d_2 x\right)^5 \phi^2 + \left(b_3 + c_3 t + d_3 x\right)^5 \phi^3\end{aligned} \tag{2.10}$$

in which the coefficients b_n, c_n and d_n $(n = 0...3)$ are the coefficients of the polynomial fit for the chemical reaction term data which are determined by polynomial fit routine in Matlab. The R_2 value was determined for the polynomial fit model for a first, second and third order polynomial in ϕ. The results are shown in Table 2.1.

Table 2.1: Results of the polynomial order fit for the chemical reaction term model

Polynomial order	Coefficients	R_2 Value
First order	A_0, A_1 both non-zero, A_2, A_3 both zero	85%
Second order	A_0, A_1, A_2 all non-zero, A_3 zero	92%
Third order	A_0, A_1 A_2, A_3 all non-zero	93%

It can be seen that increasing from a first to a second order polynomial, the $R2$ value increases with 7%. When increasing the order from two to three, the R_2 value increases with only 1%. For

this reason, a third order polynomial in ϕ will be used in this thesis. Increasing the order is not likely to improve the model accuracy dramatically and increases the computational costs.

Chapter 3

Large Eddy Simulation formulations

The basis of traditional filter-bases Large Eddy Simulation is the application of a filter in order to obtain scale separation. However, the application of filters may impose problems due to commutation errors of the spatial derivative when a non-uniform mesh is used [46]. Because the Variational Multiscale Method (VMM) works with variational projections, this method avoids this problem when applied to Large Eddy Simulation. Another advantage of this method is a residual consistency In this chapter, VMM for LES will be further elaborated. The first section of this chapter shows the theoretical basis of VMM in a LES environment for the resolved and unresolved scales. In the second section, the implementation of the simplified model problem in a VMM framework is elaborated. For the simplified model problem, the resolved scale equations are presented and various models for the unresolved scales are explained. The last section presents the implementation of the Smagorinsky model in a VMM framework.

3.1 Theoretical basis of the Variational Multiscale Method

Hughes [22] introduced the variational multiscale method as a theoretical framework and developed it as a tool to solve general problems in computational mechanics [24]. VMM is used for problems with a broad range of scales, especially when standard numerical methods are not suitable. One important property of VMM is that the range of scales is divided into a predefined number of groups. For each scale group a different numerical method is developed. For VMM the two and three-scale groups have been used. However, only the two-scale group is used in this thesis as further explained in this chapter.

In Hughes [22] a decomposition of existing scales into two scale groups is assumed, referred as the resolved (or coarse) scales and unresolved (or fine) scales. In contrast to traditional LES, the separation of scales in VMM is accomplished by a variational projection, instead of a filter. The variational projection fixes the range of resolved scales, which are finite-dimensional. Once the resolved scales are fixed, the unresolved scales are also known, which is in fact all remaining

scales. In this work the influence of the unresolved scales is determined by an approximate Green's function.

A turbulent flow consists of eddies of various sizes. The energy cascade continues due to the break up of larger eddies into smaller eddies. The break up of these eddies causes an average transfer of energy from the larger eddies to the smaller eddies. This process continues until a stable eddy motion has been reached and at this point dissipation of kinetic energy takes place. Most energy exchange takes place at scales of similar size. At a given scale size, energy comes from the next larger scale size level and it is transferred to the next smaller scale size, see Fig. 3.1. Therefore, the largest and smallest scales have no direct influence on the energy transfer at intermediate scales.

A model for the unresolved (or fine) scales more realistic must contain an interaction with the resolved scales.

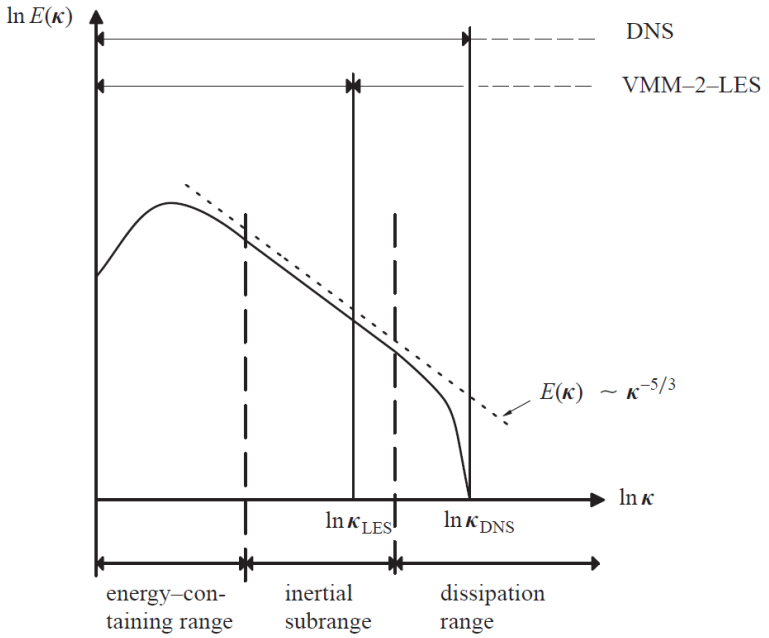

Figure 3.1: Kolmogorov energy spectrum for VMM two-scale decomposition and DNS [16]

In Hughes et al. [26] the model of the unresolved scales is driven by the residual of the resolved scales to ensure consistency. In the following section the elaboration of VMM for the simplified model problem is given, including the residual-based unresolved scale model.

3.2 VMM for the simplified model problem

The implementation of the simplified model problem in a VMM framework starts by transforming the strong form to the weak form of the Burgers, convection-diffusion (CD) and convection-

diffusion-reaction (CDR) equation. The weak form is the basis of the Variational Multiscale Method. A multiscale decomposition of the solution and weighing space is applied and variational projectors are used to describe the original weak form as two coupled non-linear problems, a coarse-scale problem and a fine-scale problem. An attempt is made to solve the fine-scale problem analytically, by assuming that the coarse scales are given by a chosen projection of the exact solution and by substituting the explicit solution of the fine-scale equation into the coarse-scale problem. In the following this is illustrated for the equations of the simplified model problem.

3.2.1 Strong form of the simplified model problem

Assume a 1D domain Ω with boundaries $\Gamma = \partial\Omega$. The strong form of the forced Burgers equation for this domain is defined as

$$\mathcal{L}u = \frac{\partial u}{\partial t} + u\frac{\partial u}{\partial x} - \nu\frac{\partial^2 u}{\partial x^2} = f_B(x,t) \tag{3.1}$$

with prescribed boundary conditions on Γ and initial condition $u(x,0) = u_0(x)$. In Eq. (3.1) u is the velocity, ν is the kinematic viscosity and $f_B(x,t)$ is the source term. It can be seen that the second term of Eq. (3.1) can be rewritten as $0.5\frac{\partial u^2}{\partial x}$, which leads to:

$$\mathcal{L}u = \frac{\partial u}{\partial t} + \frac{1}{2}\frac{\partial u^2}{\partial x} - \nu\frac{\partial^2 u}{\partial x^2} = f_B(x,t) \tag{3.2}$$

The strong form of the CD equation on the domain Ω is defined as:

$$\mathcal{L}Z = \frac{\partial Z}{\partial t} + u\frac{\partial Z}{\partial x} - D_Z\frac{\partial^2 Z}{\partial x^2} = f_{CD}(x,t) \tag{3.3}$$

with prescribed boundary conditions on Γ and initial condition $Z(x,0) = Z_0(x)$. In Eq.(3.3), Z is the mixture fraction, D_Z is the diffusive coefficient of Z and $f_{CD}(x,t)$ is the source term of the CD equation.

The strong form of the CDR equation is defined as follows:

$$\mathcal{L}\phi = \frac{\partial \phi}{\partial t} + u\frac{\partial \phi}{\partial x} - D_\phi\frac{\partial^2 \phi}{\partial x^2} = \dot{\omega} + f_{CDR}(x,t) \tag{3.4}$$

where ϕ is the progress variable, u is the velocity field, D_ϕ is the diffusion coefficient of ϕ, ω is the chemical reaction term and $f_{CD}(x,t)$ is the source term for the CDR equation. In the remainder of this section the partial derivative $\frac{\partial}{\partial x}$ will be replaced by the subscript x to denote a derivative in the x-direction.

The application of the CDR equation can be expanded using the model of the chemical source term $\dot{\omega}$, derived in Section 2.5. The strong form of the CDR equation then becomes:

$$\mathcal{L}\phi = \frac{\partial \phi}{\partial t} + u\frac{\partial \phi}{\partial x} - D_\phi\frac{\partial^2 \phi}{\partial x^2} - A_0 - A_1\phi - A_2\phi^2 - A_3\phi^3 = f_{CDR}(x,t) \tag{3.5}$$

3.2.2 Weak form of the simplified model problem

Before constructing the weak form of the simplified model problem, the trial solution space $\mathcal{V}$, $\mathcal{Z}$ and $\mathcal{P}$ and weighing function space $\mathcal{W}$ are chosen. Let these spaces be defined as:

$$u \in \mathcal{V} \subset H^1(\Omega) \tag{3.6a}$$
$$Z \in \mathcal{Z} \subset H^1(\Omega) \tag{3.6b}$$
$$\phi \in \mathcal{P} \subset H^1(\Omega) \tag{3.6c}$$
$$w \in \mathcal{W} \subset H^1(\Omega) \tag{3.6d}$$

where $H^1(\Omega)$ is the Sobolev space and it represents the space of square integrable functions together with its derivative. $L_p(\Omega)$ represents the space of functions whose power n is integrable over a domain, with n is equal or larger than 1.

The weak form of Eq. (3.1), (3.3) and (3.5) are obtained by applying the Galerkin formulation to the strong form of the equations. The Galerkin formulation can be obtained by multiplying the equations with a weighting function w and integrating over the domain Ω.

The weak form of the Burgers equation is:

Find $u \in \mathcal{V}$ such that $\forall w \in \mathcal{W}$

$$(w, \mathcal{L}u)_\Omega = (w, u_t)_\Omega + \left(w, 0.5(u^2)_x\right)_\Omega - (w, \nu u_{xx})_\Omega - (w, f_B(x,t))_\Omega \tag{3.7}$$

The weak form of the CD equation is:

Find $Z \in \mathcal{Z}$ such that $\forall w \in \mathcal{W}$

$$(w, \mathcal{L}Z)_\Omega = (w, Z_t)_\Omega + (w, uZ_x)_\Omega - (w, D_Z Z_{xx})_\Omega - (w, f_{CD}(x,t))_\Omega \tag{3.8}$$

and the weak form of the CDR equation:

Find $\phi \in \mathcal{P}$ such that $\forall w \in \mathcal{W}$

$$\begin{aligned}(w, \mathcal{L}\phi)_\Omega = (w, \phi_t)_\Omega + (w, u\phi_x)_\Omega - (w, D_\phi \phi_{xx})_\Omega \\ - \left(w, A_0 + A_1\phi + A_2\phi^2 + A_3\phi^3\right) - (w, f_{CDR}(x,t))_\Omega = 0\end{aligned} \tag{3.9}$$

with

$$(a, b)_\Omega = \int_\Omega ab \, d\Omega \tag{3.10}$$

In general, the trial solution spaces and the weighting function space do not have to span the same space. Only when the boundary conditions of u (or du/dx) are 0 and $u_0 = 0$, $\mathcal{V}$ spans the same space as $\mathcal{W}$. The same holds for Z and w and for ϕ and w.

The weak form is also known as the variational form and it will be the basis of the variational multiscale method. During this stage, no numerical approximation has been made on the weighing function and trial solution functions. This means that their spaces are of infinite size. In the next subsection, the variables are multiscale decomposed and also their solution spaces are presented.

3.2.3 Multiscale decomposition of the simplified model problem

Lets consider a multiscale decomposition into two scale groups. In terms of the weighing and trial solution spaces, the scale separation is:

$$\mathcal{V} = \overline{\mathcal{V}} \oplus \mathcal{V}' \tag{3.11a}$$
$$\mathcal{W} = \overline{\mathcal{W}} \oplus \mathcal{W}' \tag{3.11b}$$
$$\mathcal{Z} = \overline{\mathcal{Z}} \oplus \mathcal{Z}' \tag{3.11c}$$
$$\mathcal{P} = \overline{\mathcal{P}} \oplus \mathcal{P}' \tag{3.11d}$$

And multiscale decomposition of the variables yields:

$$u = \overline{u} + u' \tag{3.12a}$$
$$w = \overline{w} + w' \tag{3.12b}$$
$$Z = \overline{Z} + Z' \tag{3.12c}$$
$$\phi = \overline{\phi} + \phi' \tag{3.12d}$$

where the coarse-scale contribution is denoted with a $\overline{(..)}$ and the fine-scale contribution is denoted with a $(..)'$. In this case, the coarse-scale contribution of the weighing function space and trial solution spaces are finite-dimensional, whereas the fine-scale contribution of all spaces are infinite dimensional. The separation of scales is accomplished by choosing a projection of the exact solution onto the $\mathcal{V}$, $\mathcal{W}$, $\mathcal{Z}$ and $\mathcal{P}$ spaces. If the H_0^1 projector is chosen, then the coarse-scale variables will be nodally exact in 1D and therefore the fine-scale contributions is equal to zero on the nodes. As a result, the evaluation of the fine-scale contribution can be approximated as a local problem.

Substitution of the multiscale decomposed variables into the weak form of the Burgers, CD and CDR equation yields:

$$(\overline{w} + w', \mathcal{L}(\overline{u} + u'))_\Omega = (\overline{w} + w', f_B)_\Omega \qquad \forall \overline{w} \in \overline{\mathcal{W}}, \forall w' \in \mathcal{W}', \forall \overline{u} \in \overline{\mathcal{V}}, \forall u' \in \mathcal{V}' \tag{3.13a}$$
$$(\overline{w} + w', \mathcal{L}(\overline{Z} + Z'))_\Omega = (\overline{w} + w', f_{CD})_\Omega \qquad \forall \overline{w} \in \overline{\mathcal{W}}, \forall w' \in \mathcal{W}', \forall \overline{Z} \in \overline{\mathcal{Z}}, \forall Z' \in \mathcal{Z}' \tag{3.13b}$$
$$(\overline{w} + w', \mathcal{L}(\overline{\phi} + \phi'))_\Omega = (\overline{w} + w', f_{CDR})_\Omega \qquad \forall \overline{w} \in \overline{\mathcal{W}}, \forall w' \in \mathcal{W}', \forall \overline{\phi} \in \overline{\phi}, \forall \phi' \in \mathcal{P}' \tag{3.13c}$$

The weak form of the Burgers, CD and CDR equation (3.13a), (3.13b) and (3.13b) are linear with respect to the weighing function. Therefore one can separate Eq. (3.13) as follows:

$$(\overline{w}, \mathcal{L}\overline{u})_\Omega + (\overline{w}, \mathcal{L}u' - f_B)_\Omega - (\overline{w}, \overline{u}u')_\Omega = 0 \qquad \forall \overline{w} \in \overline{\mathcal{W}}, \forall \overline{u} \in \overline{\mathcal{V}} \tag{3.14a}$$
$$(w', \mathcal{L}\overline{u} - f_B)_\Omega + (w', \mathcal{L}u')_\Omega = 0 \qquad \forall w' \in \mathcal{W}', \forall u' \in \mathcal{V}' \tag{3.14b}$$

$$(\overline{w}, \mathcal{L}\overline{Z})_\Omega + (\overline{w}, \mathcal{L}Z' - f_{CD})_\Omega = 0 \qquad \forall \overline{w} \in \overline{\mathcal{W}}, \forall \overline{u} \in \overline{\mathcal{V}} \tag{3.15a}$$
$$(w', \mathcal{L}\overline{Z} - f_{CD})_\Omega + (w', \mathcal{L}Z')_\Omega = 0 \qquad \forall w' \in \mathcal{W}', \forall u' \in \mathcal{V}' \tag{3.15b}$$

and

$$(\overline{w}, \mathcal{L}\overline{\phi})_\Omega + (\overline{w}, \mathcal{L}\phi' - f_{CDR})_\Omega = 0 \qquad \forall \overline{w} \in \overline{\mathcal{W}}, \forall \overline{u} \in \overline{\mathcal{V}} \tag{3.16a}$$

$$(w', \mathcal{L}\overline{\phi} - f_{CDR})_\Omega + (w', \mathcal{L}\phi')_\Omega = 0 \qquad \forall w' \in \mathcal{W}', \forall u' \in \mathcal{V}' \tag{3.16b}$$

Multiscale decomposition leads to equations which are only a function of the coarse-scale contribution of w and equations which are a function of the fine-scale contribution of the weighing function w. Therefore Eq. (3.14a), (3.15a) and (3.16a) are referred as the coarse-scale equations and Equation (3.14b), (3.15b) and (3.16b) are referred as the fine-scale equations. When closely examining the results of the equation separation, it is noted that the coarse-scale equations are driven by the fine-scale contribution of u, Z and ϕ and visa versa.

At first glance, the breakdown of the original equations into a fine-scale problem and a coarse-scale problem increases the complexity of the original problem. However, if the fine-scale problem can be approximated in an intelligent manner, only a coarse-scale equation remains.

3.2.4 Fine-scale simplified model problem

The investigation of approximating the fine-scale contribution starts by looking deeper into the fine-scale equations. The fine-scale equations Eq. (3.14b), (3.15b) and (3.16b) can be expressed as:

$$(w', \mathcal{L}u')_\Omega = -(w', \mathcal{L}\overline{u} - f_B)_\Omega \tag{3.17a}$$

$$(w', \mathcal{L}Z')_\Omega = -(w', \mathcal{L}\overline{Z} - f_{CD})_\Omega \tag{3.17b}$$

$$(w', \mathcal{L}\phi')_\Omega = -(w', \mathcal{L}\overline{\phi} - f_{CDR})_\Omega \tag{3.17c}$$

Both fine-scale equations show that the fine-scale solution u', Z' and ϕ are a function of the large-scale residual $\mathcal{L}\overline{u} - f_B$, $\mathcal{L}\overline{Z} - f_{CD}$ and $\mathcal{L}\overline{\phi} - f_{CDR}$ respectively.

Because the fine-scale equations Eq.(3.17) are non-linear an approximation has to be found to solve the fine-scale variables. Scovazzi [47] provided a framework for the fine-scale approximation. In this work the relation between the fine scale solution and its residual is exploited. Under the assumption of a small fine-scale contribution compared to its coarse-scale contribution, the following asymptotic expansion can be applied:

$$V' = \epsilon V_1' + \epsilon^2 V_2' + ... = \sum_{n=1}^{\infty} \epsilon^n V_n' \tag{3.18}$$

where V' is the fine scale contribution of V, and V is the variable under consideration. ϵ is equal to the dual norm of the residual of $\overline{V}$, $\|Res(\overline{V})\|$. In summary, the asymptotic expansion of Scovazzi [47] provides a solution method to the non-linear fine-scale equations by means of a cascade of linear systems, in which the leading term is dependent on the residual of $\overline{V}$ and the other terms are dependent on the fine-scale terms V_n' of the asymptotic expansion.

Hughes [22] proposed a solution method for the fine-scale variable by solving the leading term of the linear system using the fine-scale element Green's function and the large-scale residual.

$$V'(x) = -\int_{\Omega_e} G_1'(x,x')Res(\overline{V})\, d\Omega_{x'} \tag{3.19}$$

where $G_1'(x,x')$ is a fine-scale element Green's function.

For a limited number of cases, the fine-scale element Green's function can be determined exactly. However, for complex problems the derivation of the fine-scale Green's function can be tedious or practically impossible. Therefore it is practical to approximate Eq.(3.19). In this thesis several models to approximate Eq.(3.19) are considered in order to obtain a model for the fine-scale variables. These models are presented in the next two paragraphs.

Quasi-static subscales

First approximation assumes quasi-static subscales, which means that the fine-scales are independent of time. This leads in an instantaneous response of the fine-scales to a change of the coarse scale residual [9]. When implementing the quasi-static subscales assumption, the time derivative of u', Z' and ϕ' in Eq.(3.46), Eq.(3.47) and Eq.(3.48) vanish. When using integration by parts for the viscous term of all equations and on the convective term of the Burgers equation with a boundary condition of 0, the result is:

$$\begin{aligned} &-\left(\overline{w}_x, 0.5\overline{u}^2\right)_\Omega + \left(\overline{w}_x, \overline{u}_x\right)_\Omega + \\ &\left(\overline{w}_x, -0.5(u')^2 - \overline{u}u'\right)_\Omega + \left(\overline{w}_x, \nu u_x'\right)_\Omega = \left(\overline{w}, f_B\right)_\Omega \end{aligned} \tag{3.20}$$

$$\begin{aligned} &\left(\overline{w}, \overline{u}\overline{Z}_x\right)_\Omega + \left(\overline{w}_x, D_z\overline{Z}_x\right)_\Omega + \\ &\left(\overline{w}, u'\overline{Z}_x + \overline{u}Z_x' + u'Z_x'\right)_\Omega + \left(\overline{w}_x, D_z Z_x'\right)_\Omega = \left(\overline{w}, f_{CD}\right)_\Omega \end{aligned} \tag{3.21}$$

$$\begin{aligned} &\left(\overline{w}, \overline{u}\overline{\phi}_x\right)_\Omega + \left(\overline{w}_x, D_\phi\overline{\phi}_x\right)_\Omega - \left(\overline{w}, A_0 + A_1\overline{\phi} + A_2\overline{\phi}^2 + A_3\overline{\phi}^3\right)_\Omega + \\ &\left(\overline{w}, u'\overline{\phi}_x + \overline{u}\phi_x' + u'\phi_x'\right)_\Omega + \left(\overline{w}_x, D_\phi\phi_x'\right)_\Omega - \\ &\left(\overline{w}, A_0 + A_1\phi' + A_2(\overline{\phi}\phi' + \phi'^2) + A_3(\overline{\phi}^2\phi' + \overline{\phi}\phi'^2 + \phi'^3)\right)_\Omega \\ &= \left(\overline{w}, f_{CDR}\right)_\Omega \end{aligned} \tag{3.22}$$

When the H_0^1 projector is chosen to separate the scales, the elements in the fine-scale problem has a boundary condition of 0. The next step is to approximate the Greens function shown in Eq. (3.19) by using an element-averaged fine-scale Green's function. The result is [24]:

$$u' = -\tau_u(\mathcal{L}\overline{u} - f_B) \tag{3.23a}$$
$$Z' = -\tau_Z(\mathcal{L}\overline{Z} - f_{CD}) \tag{3.23b}$$
$$\phi' = -\tau_\phi(\mathcal{L}\overline{\phi} - f_{CDR}) \tag{3.23c}$$

The algebraic operator τ can be seen as the element-averaged fine-scale Green's function. It is noted that the fine-scales u', Z' and ϕ' are driven by the residual of the coarse-scales $\overline{u}$, $\overline{Z}$ and $\overline{\phi}$ which is independent of time. Also it must be noted that Eq. (3.23a)-(3.23c) is an approximation of the fine-scale element Green's function and therefore τ can be different for each element.

The introduction of the parameter τ in a Finite Element Method problem is not new. Stabilization methods developed to assure convergence in FEM convection problems also utilizes the same parameter τ. If only one equation is considered, τ is a scalar function of u and the problem coefficients . However, if the problem consists of a system of N equations, the parameter τ is an N x N matrix.

There are numerous methods to compute the parameter τ. For the simplified model problem, the method of Hauke [18] is used, which states that the matrix τ is diagonal. This means that the fine-scale u', Z' and ϕ' is only dependent on its residual $\mathcal{L}\overline{u} - f_B$, $\mathcal{L}\overline{Z} - f_{CD}$ and $\mathcal{L}\overline{\phi} - f_{CDR}$. As a consequence, τ can be computed separately for the Burgers, CD and CDR equation.

The second model uses a different set of functions in the $\mathcal{W}'$ space. Codina [8] proposed to choose a set of functions in the $\mathcal{W}'$ space which are orthogonal to the $\overline{\mathcal{W}}$ space. When applying orthogonal subscales in the $\mathcal{W}'$ space, the fine-scale equations become:

$$u' = -\tau_u[(1 - P_{ort})(\mathcal{L}\overline{u} - f_B) - (\mathcal{L}\overline{u} - f_B)] \tag{3.24a}$$
$$Z' = -\tau_Z[(1 - P_{ort})(\mathcal{L}\overline{Z} - f_{CD})] \tag{3.24b}$$
$$\phi' = -\tau_\phi[(1 - P_{ort})(\mathcal{L}\overline{\phi} - f_{CDR})] \tag{3.24c}$$

where P_{ort} is L^2 projection onto $\overline{\mathcal{W}}$.

Dynamic subscales

The last elaborated model for the fine-scale equations uses dynamic subscales, which means that the fine-scale variables are dependent on time. This means that the coarse-scale equations Eq.(3.46) Eq.(3.47) and Eq.(3.48) have to be solved when dynamic subscales are assumed. In the work of Codina et al. [9], dynamic subscales are only used in combination with orthogonal subscales and the fine-scale models are given as:

$$\frac{\partial u'}{\partial t} = -(1 - P_{ort})(\mathcal{L}\overline{u} - f_B) - \frac{u'}{\tau_u} \tag{3.25a}$$
$$\frac{\partial Z'}{\partial t} = -(1 - P_{ort})(\mathcal{L}\overline{Z} - f_{CD}) - \frac{Z'}{\tau_Z} \tag{3.25b}$$
$$\frac{\partial \phi'}{\partial t} = -(1 - P_{ort})(\mathcal{L}\overline{\phi} - f_{CDR}) - \frac{\phi'}{\tau_\phi} \tag{3.25c}$$

In order to determine the fine-scale variables u', Z' and ϕ', both explicit and implicit methods can be used.

When an explicit in time is used, the fine-scale variables are determined by:

$$(u')^{n+1} = -(u')^n + \Delta t \frac{\partial (u')}{\partial t}^n \tag{3.26a}$$

$$(Z')^{n+1} = -(Z')^n + \Delta t \frac{\partial (Z')}{\partial t}^n \tag{3.26b}$$

$$(\phi')^{n+1} = -(\phi')^n + \Delta t \frac{\partial (\phi')}{\partial t}^n \tag{3.26c}$$

This is referred to as the lagging model.

When an implicit method in time is used, the fine-scale variables are determined by:

$$(u')^{n+1} = -(u')^n + \Delta t \frac{\partial (u')}{\partial t}^{n+1} \tag{3.27a}$$

$$(Z')^{n+1} = -(Z')^n + \Delta t \frac{\partial (Z')}{\partial t}^{n+1} \tag{3.27b}$$

$$(\phi')^{n+1} = -(\phi')^n + \Delta t \frac{\partial (\phi')}{\partial t}^{n+1} \tag{3.27c}$$

This is referred to as the leading model.

τ definitions for the simplified model problem

In this paragraph several definitions of τ are presented in order to approximate the fine-scale element Green's function. The first presented τ definition is from Shakib et al. [48]. In this paper, the following definition is proposed:

$$\tau_{st}^{sh} = \frac{1}{\sqrt{9\left(\frac{4D}{h^2}\right)^2 + \left(\frac{2u}{h}\right)^2}} \tag{3.28}$$

where D is the kinematic viscosity ν or diffusivity D_z when considering the Burgers equation or the CD equation respectively. It is claimed that a local truncation error analysis reveals fourth-order accuracy [48]. Navarro Hernandez [33] optimized the coefficients of Eq. (3.28) using the Burgers equation to model a channel flow. These improvements are also used for the τ definition corresponding to the CD equation. The improved variant reads:

$$\tau_{NH}^{sh} = \frac{1}{\sqrt{4u^2/h^2 + 150D^2/h^4}} \tag{3.29}$$

where D is the kinematic viscosity ν or diffusivity D_z when considering the Burgers equation or the CD equation respectively. Both variants can also be used for the CDR equation

$$\tau_{\phi}^{sh} = \frac{1}{\sqrt{4u^2/h^2 + c_1 D_{\phi}^2/h^4 + |s|^2}} \tag{3.30}$$

where c_1 is a coefficient, which is 144 for Shakib's definition or 150 for the Adjusted Shakib's definition by Navarro. s is a measure of the source term which is derived later.

Hauke and Garcia-Olivares [19] performed a study relating to the definition of τ for the CD equation. The investigated τ originates from the standard design for τ which comes from advection-diffusion theory and is defined as follows:

$$\tau_{ad} = \frac{h}{2|\vec{u}|}\tilde{\xi}(\alpha) \tag{3.31}$$

where $\tilde{\xi}(\alpha)$ is derived from imposing nodal exactness, which leads to:

$$\tilde{\xi}(\alpha) = \coth\,\alpha - \frac{1}{\alpha} \approx \min\left(\frac{1}{3}\alpha, 1\right) \tag{3.32}$$

where

$$\alpha = \frac{|\vec{u}|h}{2D} \tag{3.33}$$

In the work of Hauke and Garcia-Olivares [19], several versions of τ are for the CDR equation are presented. The first τ is obtained by Codina [7], which originates from the maximum principle. Originally this expression for τ is only valid for a negative source term, but the expression is extended to include positive source terms. The definition is:

$$\tau_{\phi}^{Cod} = \frac{1}{\frac{4D_{\phi}}{h^2} + \frac{2\vec{u}}{h} + |s|} \tag{3.34}$$

where D_{ϕ} is the diffusivity corresponding to the CDR equation. This definition can also be used for the CD equation when the source term s is set to 0.

From convergence and stability theory, Franca and Valentin [14] obtained another expression for negative source terms. Also this equation is extended for all s by Hauke [18]:

$$\tau_{\phi}^{Fv} = \frac{1}{\frac{2D_{\phi}}{m_k h^2}\max(1, Pe_2) + |s|\max(1, Pe_1)} \tag{3.35}$$

where

$$Pe_1 = \frac{2D_{\phi}}{m_k|s|h^2} \tag{3.36}$$

and

$$Pe_2 = \frac{m_k|\vec{u}|h}{D_{\phi}} \tag{3.37}$$

m_k is $1/3$ for linear elements and in practice also for bilinear elements.

The definition of τ proposed by Franca and Valentin [14] can also be used for the Burgers and CD equation when the limit of parameter s is going to zero, yielding:

$$\tau^{Fv} = \frac{1}{\frac{2D}{m_k h^2}\max(1, Pe_2) + \frac{2D}{m_k h^2}} \tag{3.38}$$

where D is the kinematic viscosity ν or diffusivity D_z when considering the Burgers equation or the CD equation respectively.

In the definition of τ corresponding to the CDR equation assumes that the source term $\dot{\omega}$ can be written as $\dot{\omega} = s\phi$, resulting in the following operator:

$$\mathcal{L}\phi = \phi_t u\phi_x - D_\phi \phi_{xx} - s\phi \rightarrow \mathcal{L} = (..)_t + u(..)_x - D_\phi(..)_{xx} - s \tag{3.39}$$

In this thesis, the source term is approximated by a third order polynomial. To use the previous mentioned τ_ϕ in this paragraph, a suitable expression for s has to be found. Expanding Eq. (3.23c) and rearranging this equation and neglecting the time derivative of ϕ'_t results in:

$$\begin{aligned} &-\left[\left(w', (\overline{u}+u')\overline{\phi}_x\right)_\Omega - \left(w', D_\phi \overline{\phi}_{xx}\right)_\Omega - \left(w', A_3\overline{\phi}^3 + A_2\overline{\phi}^2 + A_1\overline{\phi} + A_0\right)_\Omega\right] = \\ &\left(w', (\overline{u}+u')\phi'_x\right)_\Omega - \left(w', D_\phi \phi'_{xx}\right)_\Omega - \left(w', 3A_3\overline{\phi}^2\phi' + 2A_2\overline{\phi}\phi' + A_1\phi'\right)_\Omega \end{aligned} \tag{3.40}$$

The first term of (3.23c) shows that the L_2 product is taken from w' and the linear operator $\mathcal{L}$ which acts only on ϕ'. When this is compared to the second line of (3.40), and substituting $(\overline{u}+u') = u$, the result is:

$$\left(w', u\phi'_x\right)_\Omega - \left(w', D_\phi \phi'_{xx}\right)_\Omega - \left(w', (3A_3\overline{\phi}^2 + 2A_2\overline{\phi} + A_1)\phi'\right)_\Omega = \left(w', \mathcal{L}\phi'\right)_\Omega \tag{3.41}$$

Taking the linear operator defined in (3.39) and compare with the expression above, s is:

$$s = 3A_3\overline{\phi}^2 + 2A_2\overline{\phi} + A_1 \tag{3.42}$$

The expression above for s is implemented if τ needs to be determined for the CDR equation.

3.2.5 Coarse-scale simplified model problem

The coarse-scale equations are obtained by substituting the approximation of the fine-scale equations (3.23) into the coarse-scale equations of the Burgers, CD and CDR Eq.(3.14a), (3.15a) and (3.16a). To continue further in the elaboration of the coarse-scale equations, a remark has to be made about the implication of substituting the fine-scale equations into the coarse-scale equations.

In Subsection 3.2.4, it is stated that the fine-scale equation contains an approximation of the element fine-scale Green's function and therefore this approximation is assumed to be only valid in the element interior. As a consequence, all inner products with fine-scale approximation contributions are integrated by parts. This results that potential derivatives of the fine-scale approximation are transferred to the weighing functions. Because the fine-scale approximations are smooth in the element interior, the derivative of the weighting function is well-defined in the element interior. This interpretation of the multiscale method follows from the methodology presented in the work of Calo [6] and Hughes [22], only the approximation of the fine-scale solution differs.

When implementing the presented methodology, the implemented coarse-scale contribution of the simplified model problem can be obtained. The first step of the process is to merge the first term and the second term of Eq. (3.14a), (3.15a) and (3.16a) and substituting the strong form of the representative Eq. (3.1, 3.3 and 3.4) into the weak form. For the Burgers equation, this results in:

$$\begin{aligned}&\big(\overline{w}, \mathcal{L}(\overline{u}+u')\big)_\Omega = \\ &\big(\overline{w}, (\overline{u}+u')_t\big)_\Omega - \big(\overline{w}_x, 0.5(\overline{u}+u')^2\big)_\Omega - \big(\overline{w}, \nu(\overline{u}+u')_{xx}\big)_\Omega = (\overline{w}, f_B)_\Omega\end{aligned} \tag{3.43}$$

For the CD equation, this results in:

$$\begin{aligned}&\big(\overline{w}, \mathcal{L}(\overline{Z}+Z')\big)_\Omega = \\ &\big(\overline{w}, (\overline{Z}+Z')_t\big)_\Omega + \big(\overline{w}, (\overline{u}+u')(\overline{Z}+Z')_x\big)_\Omega - \big(\overline{w}, D_Z(\overline{Z}+Z')_{xx}\big)_\Omega = (\overline{w}, f_{CD})_\Omega\end{aligned} \tag{3.44}$$

And for the CDR equation, the result is:

$$\begin{aligned}&\big(\overline{w}, \mathcal{L}(\overline{\phi}+\phi')\big)_\Omega = \\ &\big(\overline{w}, (\overline{\phi}+\phi')_t\big)_\Omega + \big(\overline{w}, (\overline{u}+u')(\overline{\phi}+\phi')_x\big)_\Omega - \big(\overline{w}, D_\phi(\overline{\phi}+\phi')_{xx}\big)_\Omega = \\ &\big(\overline{w}, A_0 + A_1(\overline{\phi}+\phi') + A_2(\overline{\phi}+\phi')^2 + A_3(\overline{\phi}+\phi')^3\big)_\Omega + (\overline{w}, f_{CDR})_\Omega\end{aligned} \tag{3.45}$$

Applying integration by parts on the third term and rearranging the Burgers Eq.(3.43) gives the implemented coarse-scale contribution of the Burgers equation:

Find $\overline{u} \in \mathcal{V}$, such that $\forall \overline{w} \in \overline{\mathcal{W}}$:

$$\begin{aligned}&(\overline{w}, \overline{u}_t)_\Omega - \big(\overline{w}, 0.5\overline{u}^2\big)_\Omega + (\overline{w}_x, \nu\overline{u}_x)_\Omega + \\ &\big(\overline{w}, u'_t - 0.5(u')^2 - \overline{u}u'\big)_\Omega + \big(\overline{w}_x, \nu u'_x\big)_\Omega = (\overline{w}, f_B)_\Omega \qquad \forall \overline{w} \in \overline{\mathcal{W}}, \quad \forall \overline{u} \in \overline{\mathcal{V}}\end{aligned} \tag{3.46}$$

First line of Eq.(3.46) shows the L_2 products of the coarse-scale weighing function $\overline{w}$ and the coarse-scale velocity $\overline{u}$ and/or its derivatives. When it is compared with Eq.(3.7), it can be seen that they are almost identical. The only difference is that the weak form acts on the coarse and fine scale variables and weighing function, whereas the first line of (3.46) involves the coarse-scale variables and the coarse-scale weighing function. The second line of Eq.(3.46) shows the interaction between the fine scales and the coarse scales.

To obtain the coarse-scale contribution of the CD equation the same procedure as for the Burgers equation is applied. Again neglecting the time derivative of the fine-scale contribution, integration of parts of the third term of Eq.(3.44) and rearranging gives:

Find $\overline{Z} \in \mathcal{Z}$, such that $\forall \overline{w} \in \overline{\mathcal{W}}$:

$$\begin{aligned}&\big(\overline{w}, \overline{Z}_t\big)_\Omega + \big(\overline{w}, \overline{u}\overline{Z}_x\big)_\Omega + \big(\overline{w}_x, D_z\overline{Z}_x\big)_\Omega + \\ &\big(\overline{w}, Z'_t + u'\overline{Z}_x + \overline{u}Z'_x + u'Z'_x\big)_\Omega + \big(\overline{w}_x, D_z Z'_x\big)_\Omega = (\overline{w}, f_{CD})_\Omega \qquad \forall \overline{w} \in \overline{\mathcal{W}}, \quad \forall \overline{Z} \in \overline{\mathcal{Z}}\end{aligned}$$

(3.47)

When the first line of Eq.(3.47) is compared with Eq.(3.8), it can be clearly seen that both are nearly identical. The only difference is that the weak form acts on the coarse and fine scale variables and weighing function, but the first line of Eq.(3.47) acts on the coarse-scale counterparts. The second line of Eq.(3.47) shows the behaviour of the fine-scales on the coarse-scales.

To obtain the coarse-scale contribution of the CDR equation the same procedure as for the Burgers equation is applied. Again neglecting the time derivative of the fine-scale contribution, integration of parts of the third term of Eq.(3.45) and rearranging gives:

Find $\overline{\phi} \in \mathcal{P}$, such that $\forall \overline{w} \in \overline{\mathcal{W}}$:

$$\begin{aligned}
&\left(\overline{w}, \overline{\phi}_t\right)_\Omega + \left(\overline{w}, \overline{u}\overline{\phi}_x\right)_\Omega + \left(\overline{w}_x, D_\phi \overline{\phi}_x\right)_\Omega - \left(\overline{w}, A_0 + A_1\overline{\phi} + A_2\overline{\phi}^2 + A_3\overline{\phi}^3\right)_\Omega + \\
&\left(\overline{w}, \phi'_t + u'\overline{\phi}_x + \overline{u}\phi'_x + u'\phi'_x\right)_\Omega + \left(\overline{w}_x, D_\phi \phi'_x\right)_\Omega - \\
&\left(\overline{w}, A_0 + A_1\phi' + A_2(\overline{\phi}\phi' + \phi'^2) + A_3(\overline{\phi}^2\phi' + \overline{\phi}\phi'^2 + \phi'^3)\right)_\Omega \\
&= (\overline{w}, f_{CDR})_\Omega \qquad\qquad \forall \overline{w} \in \overline{\mathcal{W}}, \quad \forall \overline{\phi} \in \overline{\mathcal{P}}
\end{aligned} \tag{3.48}$$

When the first line of Eq.(3.48) is compared with the weak form Eq.(3.9), it can be clearly seen that both are nearly identical. The only difference is that the weak form acts on the coarse and fine scale variables and weighing function, but the first line of Eq.(3.48) acts on the coarse-scale counterparts. The second and third line of Eq.(3.48) shows the effect of the fine scales on the coarse scales.

3.3 Smagorinsky for the simplified model problem

A popular method to model the fine scales in a LES problem is to use an eddy-viscosity model. With such a model the turbulent stress term is related to the gradient of the coarse scale flow to close the system of equations.

$$\tau_{ij}^{tur} = \nu_T \left(\frac{\partial u_i}{\partial x_j} + \frac{\partial u_j}{\partial x_i} \right) + \frac{2}{3} k \delta_{ij} \tag{3.49}$$

where ν_T is the turbulent eddy viscosity, τ_{ij}^{tur} is the turbulent stress term, k is the turbulent kinetic energy and δ_{ij} is the Kronecker delta.

When Eq. (3.49) is implemented in Eq. (3.46) and omitting the fine-scale contributions, the result is: Find $\overline{u} \in \mathcal{V}$, such that $\forall \overline{w} \in \overline{\mathcal{W}}$:

$$\left(\overline{w}, \overline{u}_t\right)_\Omega - \left(\overline{w}, 0.5\overline{u}^2\right)_\Omega + \left(\overline{w}_x, (\nu + \nu_t)\overline{u}_x\right)_\Omega = (\overline{w}, f_B)_\Omega \qquad \forall \overline{w} \in \overline{\mathcal{W}}, \quad \forall \overline{u} \in \overline{\mathcal{V}} \tag{3.50}$$

The eddy viscosity approach can also be applied for the CD and CDR equation. The eddy diffusivity K of the mixture fraction and progress variable are related to the eddy viscosity ν_T via the turbulent Schmidt number $Sc_t = {}^{\nu_T}/_{K}$. When Eq. (3.49) and the turbulent Schmidt number are implemented in Eq. (3.47) and in Eq. (3.48) and omitting the fine-scale contributions, the result is:

$$\left(\overline{w}, \overline{Z}_t\right)_\Omega + \left(\overline{w}, \overline{u}\overline{Z}_x\right)_\Omega + \left(\overline{w}_x, \left(D_z + \frac{\nu_T}{Sc_t}\right)\overline{Z}_x\right)_\Omega = \left(\overline{w}, f_{CD}\right)_\Omega \qquad \forall \overline{w} \in \overline{\mathcal{W}}, \quad \forall \overline{Z} \in \overline{\mathcal{Z}} \tag{3.51}$$

$$\begin{aligned}&\left(\overline{w}, \overline{\phi}_t\right)_\Omega + \left(\overline{w}, \overline{u}\overline{\phi}_x\right)_\Omega + \left(\overline{w}_x, \left(D_\phi + \frac{\nu_T}{Sc_t}\right)\overline{\phi}_x\right)_\Omega - \left(\overline{w}, A_0 + A_1\overline{\phi} + A_2\overline{\phi}^2 + A_3\overline{\phi}^3\right)_\Omega \\ &= \left(\overline{w}, f_{CDR}\right)_\Omega \qquad\qquad \forall \overline{w} \in \overline{\mathcal{W}}, \quad \forall \overline{\phi} \in \overline{\mathcal{P}}\end{aligned} \tag{3.52}$$

When the Smagorinsky model is used for a 1D flow, the eddy viscosity can be expressed as:

$$\nu_t = C_s^2 h^2 \left(\frac{du}{dx}\frac{du}{dx}\right)^{1/2} \tag{3.53}$$

where C_s is the Smagorinsky constant and h is the element size.

The Smagorinsky model was introduced in the unresolved scale equations to account for the dissipation of the missing small scales. However, the Smagorinsky model does not replace any unclosed terms, but it increases dissipation on the small scales.

Chapter 4

Method of Manufactured Solutions results

The method of manufactured solutions (MMS) provides a procedure for code verification. The idea of this method is to select exact solutions (or manufactured solutions) for the chosen variables a priori without being disturbed about the physical context of the governing equations. With the selected exact solution the corresponding analytical source terms are generated by substituting the solution into the governing equations. The equations are solved on multiple computational grids with a different number of elements using the derived source terms. With the results, the performance of several features are evaluated, namely to check if the coding is done correctly, identify the behaviour of potential errors when the wave number is altered, determining the global discretisation error in the numerical solutions and to identify the performance of several fine-scale models.

The manufactured solution must meet the following conditions [45]:

- The solutions must be continuous
- Each manufactured solution must be continuously differentiable up to the order of corresponding terms in the governing equations and the result of differentiation must be non-zero
- The manufactured solutions should avoid negative values for quantities which are physically always positive, for example time, temperature and pressure.

In this thesis, also the influence of the wave number to the global discretisation error is evaluated. Therefore the following manufactured solution $\psi(x,t)$ is chosen:

$$\psi(x,t) = \psi(0) + sin\left(\frac{2\pi cx}{L}\right) sin^2(t) \tag{4.1}$$

where ψ is the considered variable (velocity u, mixture fraction Z or progress variable ϕ) c is the wave number, L is the length of the domain and p_0 is the initial condition. When implementing Eq.(4.1) into Eq.(3.5), the source term of the manufactured solutions are obtained.

4.1 Setup method of manufactured solution test-case

The goals of the MMS test case is to identify the performance of several fine-scale models and to identify potential errors. To achieve these goals, various fine-scale models are tested of the velocity u and the velocity profile and error plot are analysed. The following fine-scale models are considered in the MMS test case:

- No model
- Smagorinsky
- VMM with quasi-static subscales

For each of the VMM models, all the presented τ explained in paragraph 3.2.4 are implemented on a one dimensional mesh with a length of $0.15\,\mathrm{m}$ and a run time of $0.15\,\mathrm{s}$.

Table 4.1 shows the other parameters corresponding to the MMS test case. The test cases are

Table 4.1: MMS test case parameters

Symbol	Parameter	Value
u_0	Initial velocity	$1\,\mathrm{m/s}$, $6\,\mathrm{m/s}$
C_s	Smagorinsky coefficient	0.18
ν	Kinematic viscosity	$1.56 \times 10^{-5}\,\mathrm{m^2/s}$

performed on the HPC12 server using the in-house program Mex , which uses a number of existing C++ class libraries.

4.2 MMS test case results

This section shows the results of the MMS test case. This consist of an instantaneous plot for the lowest possible number of elements and an error plot for all elements for a selected number of wave numbers. Because the $H1$ projection is chosen and linear trial and weighing functions are used, the error of u is computed at the nodes as:

$$\epsilon = u_{predicted} - u_{exact} \tag{4.2}$$

The error plot u for wave number is 1 and for $u_0 = 1$ is shown in Figure 4.1.

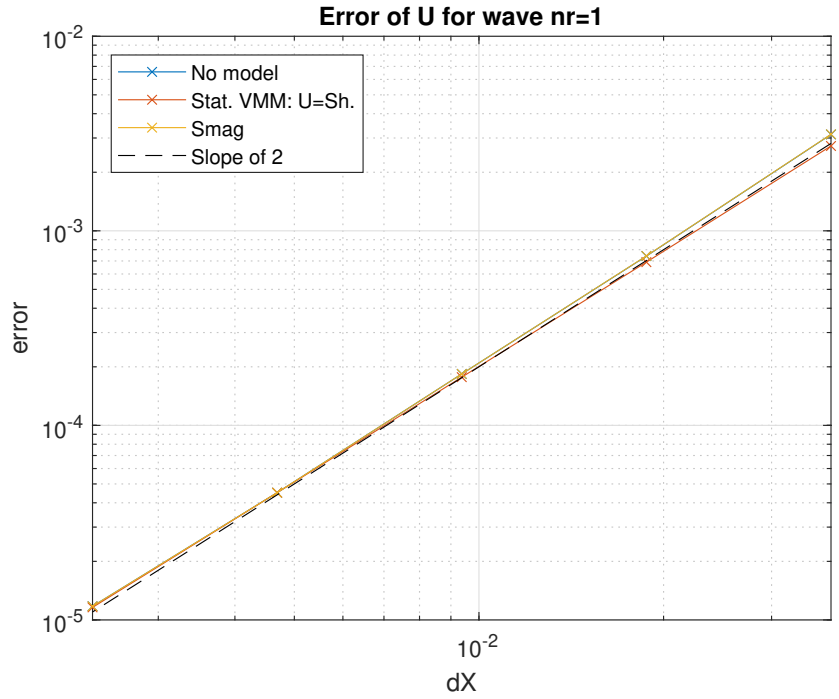

Figure 4.1: Error plot u for wave number $= 1$ and $u_0 = 1$

When analysing Figure 4.1, it is observed that the slope of the three methods is equal to 2, which indicates that the order of accuracy of the three considered fine-scale models is 2. This is consistent the chosen basis function (piecewise-linear) and the chosen time march scheme (Generalized Alpha).

The next step is to investigate the instantaneous velocity profile. For this analysis the instantaneous velocity profiles for an initial velocity of $1\,\mathrm{m/s}$ and for $N = 5$ and $N = 7$ are generated, where N is the number of elements. The results are presented in Figure 4.2.

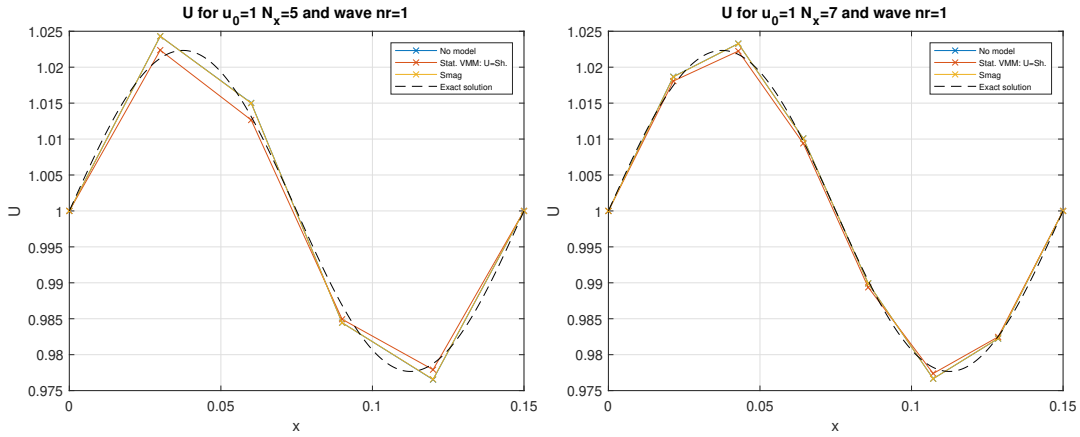

Figure 4.2: Instantaneous u results for $u_0 = 1$, $N = 5$ (left) and $N = 7$ (right)

In Figure 4.2, only the τ_U formulation of Shakib (Eq. (3.28)) is shown. Changing τ_U has a negligible effect on the results. When analysing the results, it is observed that the instantaneous velocity profile is asymmetric when using VMM for N=5 and N=7, whereas the no-model and Smagorinsky results are symmetric. The asymmetry is significantly at $x = 0.075$.

The level of asymmetry decreases when increasing the number of elements. To analyse the observed asymmetry in detail, similar instantaneous velocity plots are generated for an initial velocity of $6\,\mathrm{m/s}$. These plots are presented in Figure 4.3.

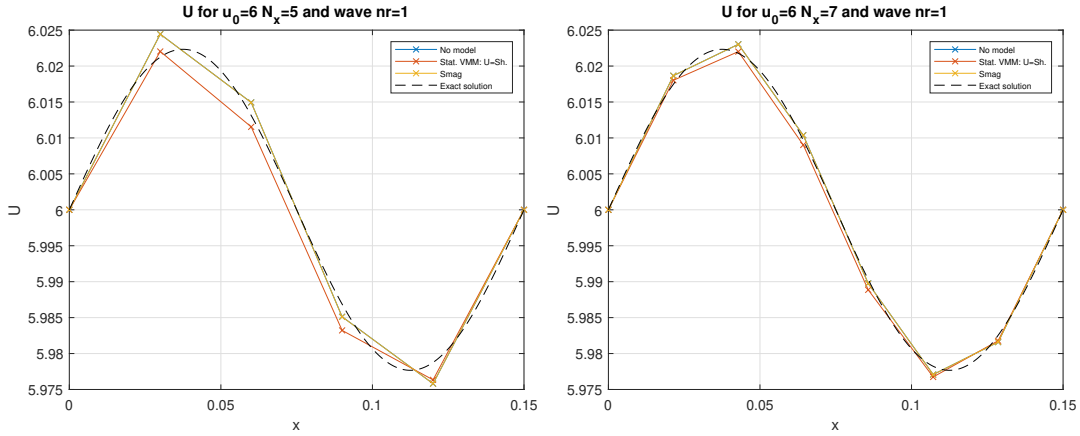

Figure 4.3: Instantaneous u results for $u_0 = 6$, $N = 5$ (left) and $N = 7$ (right)

When analysing Figure 4.3, it is observed that the instantaneous velocity profile is still asymmetric when using VMM for N=5 and N=7, and that the level of asymmetry is higher when $u_0 = 6\,\mathrm{m/s}$ comparing to the level of asymmetry when $u_0 = 1\,\mathrm{m/s}$. This behaviour is not expected. The Burgers equation is Galilean invariant, which means in this test case a shift in the initial condition will lead to an equal shift in the results. The latter can be seen for the Smagorinsky and the no model results.

A potential source of the VMM discrepancy could be the definition of u'. When investigating the fine-scale Eq. (3.23), it is observed that the fine-scale contribution of u is dependent on the residual of the Burgers equation and on τ_U. As the Burgers equation is Galilean invariant, its residual must be Galilean invariant as well. The other potential error source is the definition of τ_U. When analysing Paragraph 3.2.4, it is observed that τ for the velocity and for the CD and CDR equation are dependent on a reference velocity u. In the source code, u in the τ equations is set as the velocity on the integration point. When a shift is introduced in the MMS initial condition, the velocity which is input for τ increases as well. This is an undesirable mechanism, as this leads to a u' (and also Z' and ϕ') which is not Galilean invariant.

Therefore the definition of τ should be adjusted as such that it's Galilean invariant. This is further elaborated in the next section.

4.3 MMS test case results with a Galilean invariant τ

In order to adjust the τ such that it's Galilean invariant, u will be replaced by $\tilde{u}$, which is defined as:

$$\tilde{u} = u - u_{ref} \tag{4.3}$$

In the MMS test case, u_{ref} is taken as u_0. For the analysis of the instantaneous velocity profile u_0 is taken as $6\,\mathrm{m/s}$ and the profiles are generated for $N = 5$ and $N = 7$. The results are shown in Figure 4.4.

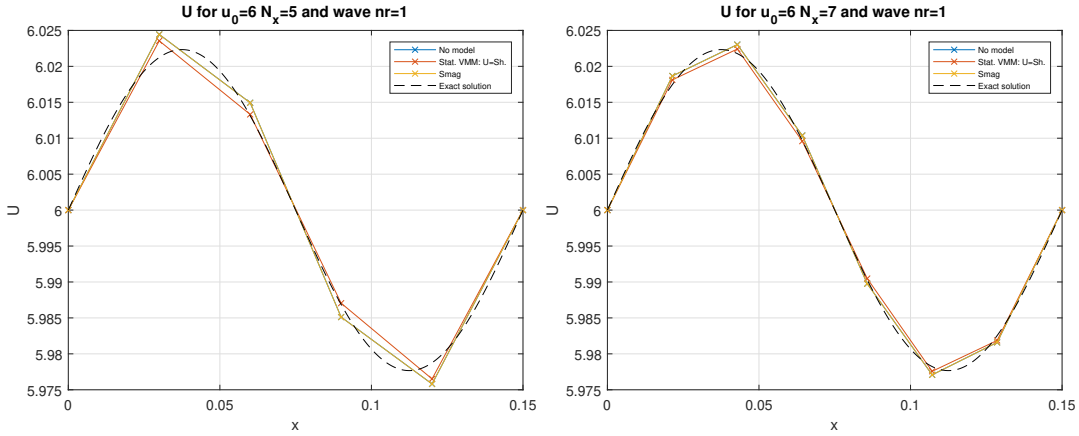

Figure 4.4: Instantaneous u results which adjusted τ for $u_0 = 6$, $N = 5$ (left) and $N = 7$ (right)

When comparing Figure 4.4 and Figure 4.3, it is observed that the asymmetry around $x = 0.075$ has vanished when a Galilean invariant τ is applied. With a Galilean invariant τ, u' is also Galilean invariant.

Chapter 5

Simplified model problem reference results

The simplified model problem (SMP) contains the important aspects of turbulent non-premixed combustion. To analyse the simplified model problem, a suitable test case must be chosen, which is in this case a turbulent non-premixed combustion jet flame. The setup of the test case is further discussed in the first section. Before presenting the results, first an estimation of the error in space and time reference case has to be determined, which is shown in the second section. The third section contains the results of the SMP test case. The last section describes the performance of the SMP test case compared with a full 3D turbulent non-premixed combustion jet flame.

5.1 Setup of the SMP reference test case

One of the important aspects of the simplified model problem are the forcing functions. These functions are be generated from LES results of a 3D turbulent non-premixed combustion jet flame problem. For this thesis, the OpenFOAM LES code of Klaessen [30] is used. This code is used to model the Delft-Jet in Hot-Coflow (DJHC), which describes a round turbulent non-premixed combustion jet flame accompanied by a pilot flame. For the purpose of the SMP test case, results are generated of a non-premixed jet flame without a pilot flame for the construction of the appropriate forcing term and other relevant data.

The collection of the relevant data started with running a 3D LES calculation using a non-uniform mesh with 201 nodes in x-direction, 48 nodes in radial direction and 36 nodes in azimuthal direction. The spacing between the nodes on the centerline in x-direction was at its lowest next to the inlet and increases when moving downstream. The relevant data was extracted using 201 probe points which were located on the nodes on the centerline. The purpose of the probe points was to retrieve the forcing terms f_u, f_Z and f_ϕ, velocity u, mixture fraction Z and progress variable ϕ at every time step and to store the acquired data in a database. For the LES calculations a time step of $5 \times 10^{-6}\,\mathrm{s}$ was used.

Next step is to post-process the generated data into a suitable form. The following properties have to be taken into account when post-processing the data:

- The SMP test case uses a uniform grid
- Due to the Nyquist theorem, the extracted variables shall not contain more than $^{N_{min}}/_{2}$ points in x-direction and $^{N_t}/_{2}$ points in time. N_{min} is the smallest number of elements considered in the SMP test case and N_t is the number of time steps in the SMP test case

This can be achieved by applying a Fourier transform and extract the lowest $^{N_{min}}/_{4}$ frequencies in x-direction and the lowest $^{N_t}/_{2}$ frequencies in the time domain.

The post-processed data is also to impose the boundary conditions and initial conditions for u, Z and ϕ. The boundary conditions can be extracted from the results of u, Z and ϕ for $x = 0$. At the other boundary, a non reflecting boundary condition is imposed. The initial conditions are extracted when t is $0.15\,\mathrm{s}$. From this time u is always greater than 0. When u is positive, information only enters the domain allowing to specify the three variables at $x = 0$.

Other relevant properties of the SMP reference test case are presented in Table 5.1. For a round

Table 5.1: Relevant parameters SMP reference test case

Description	Value
Length of domain in x-direction	$0.15\,\mathrm{m}$
Starting time	$0.15\,\mathrm{s}$
Start averaging time	$0.3\,\mathrm{s}$
End time	$0.45\,\mathrm{s}$
Time step	$5 \times 10^{-6}\,\mathrm{s}$
Kinematic viscosity	$1.56 \times 10^{-5}\,\mathrm{m^2/s}$
Diffusivity of Z	$1.4 \times 10^{-5}\,\mathrm{m^2/s}$
Diffusivity of ϕ	$1.4 \times 10^{-5}\,\mathrm{m^2/s}$
Smagorinsky coefficient	0.17
Turbulent Schmidt number	0.9

jet a Smagorinsky coefficient of 0.17 is recommended by Pope [43] and verified by Ilyushin and Krasinsky [27]. The turbulent Schmidt number is defined as the ratio of the eddy viscosity and the eddy diffusivity of Z and ϕ. The value of 0.9 is also used in the work of Klaessen [30].

As shown in Chapter 4, using a Galilean invariant τ improves the results significantly. Therefore a Galilean invariant formulation for τ_u, τ_Z and τ_ϕ is used, which means that the transformation described in Eq. (4.3) has to be applied. For the SMP test case u_{ref} is set as $7\,\mathrm{m/s}$, which is the average velocity at $x = 0$.

The SMP reference test cases uses no fine-scale model, but different meshes. The chosen reference case is compared to the OpenFOAM reference case. The SMP reference test cases are performed on the HPC12 server using the in-house program MEX, which uses a number of existing C++

class libraries for FEM applications. Linear basis functions are used and for the time march scheme the Generalized alpha scheme is chosen.

5.2 Error estimation study of the reference case

The error estimation in space and time is executed using Richardson extrapolation. This method provides an estimation of the error which is independent of the chosen discretisation method. The error estimate starts with obtaining the observed order of accuracy p_0.

Let f_1 be a value of a simple function of the discrete solution with step size h_1, where h_1 can be Δt or Δx. Consider a solution f_2 of a coarser mesh with step size h_2, which is related to h_1 as:

$$r = \frac{h_2}{h_1} \tag{5.1}$$

For the determination of the observed order of accuracy the solution f_3 of another coarser mesh with step size h_3 is needed. The step size h_3 is related to the step size h_2 as described in Eq. (5.1). The values f_1, f_2 and f_3 can be expressed in terms of the exact value f_e as:

$$f_1 = f_e + ah^{p_0} + \mathcal{O}(h^{p_0+1}) \tag{5.2a}$$
$$f_2 = f_e + a(rh)^{p_0} + \mathcal{O}((rh)^{p_0+1}) \tag{5.2b}$$
$$f_3 = f_e + a(r^2h)^{p_0} + \mathcal{O}((r^2h)^{p_0+1}) \tag{5.2c}$$

where a is a function of the gradient of the continuous solution.

When neglecting the higher order terms, the observed order of accuracy can be determined by:

$$p_0 = \frac{ln\left(\frac{f_3-f_2}{f_2-f_1}\right)}{ln(r)} \tag{5.3}$$

With the observed order of accuracy, the error can be estimated, which is a function of the step size. It is noted that Eq. (5.3) is only valid in the asymptotic region. In this region the higher order terms of the truncation error is small compared to the leading error term. Another approach to demonstrate the validity of Eq. (5.3) is to show that the expected order of accuracy p is equal to the observed order of accuracy p_0. With the observed order of accuracy the error can be estimated using $\epsilon \approx h^{p_0}$.

In order to estimate the error in space and time for the SMP test case, the presented methodology is executed. First step is to define 3 grids for the estimation of the error in space and 3 grids for the estimation of the error in time. The following grids presented in Table 5.2 are used for the error estimation. The error estimation in space and time is based on the calculated mean value of Z. Figure 5.1 shows the observed order of accuracy of x when Eq. (5.3) is applied on the Z results of grid G1, G2 and G3.

Table 5.2: Used grids for the error estimation in space and time

Grid	Number of elements	Number of time steps	Application
G1	800	6×10^4	Error estimation in space
G2	1000	6×10^4	Error estimation in space
G3	1250	6×10^4	Error estimation in space
GT1	400	6×10^4	Error estimation in time
GT2	400	1.2×10^5	Error estimation in time
GT3	400	2.46×10^5	Error estimation in time

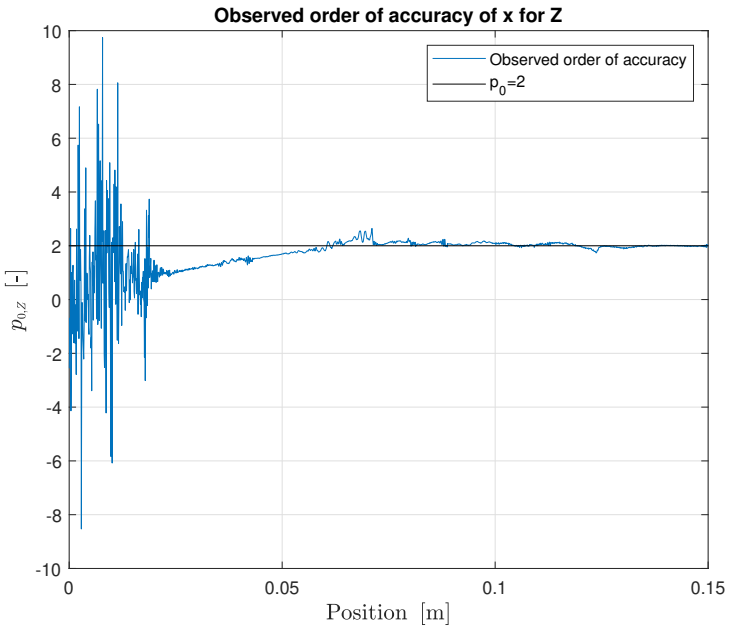

Figure 5.1: Observed order of accuracy of x for the mixture fraction

Because linear basis functions are used, the expected order of accuracy is 2. When analysing Figure 5.1, it is observed that the observed order of accuracy is equal to 2 between x=$0.075\,\mathrm{m}$ and x=$0.15\,\mathrm{m}$. From x=$0.025\,\mathrm{m}$ to x=$0.075\,\mathrm{m}$, the observed order of accuracy is slowly progressing from 1 to 2. From x=$0\,\mathrm{m}$ to $0.025\,\mathrm{m}$ the observed order of accuracy is oscillating. A possible reason for this behaviour is due to the file data truncation error of the results files. The results of the simulations are stored to 5 decimal places. When the difference between the results approaches 0, their ratio cannot be determined accurately. This is observed in Figure 5.2, as the differences between the results approaches 0. The file data truncation errors are introduced in Eq. (5.3) which leads to unrealistic values of the order of accuracy near x is $0\,\mathrm{m}$ and slowly progressing to its true order of accuracy value.

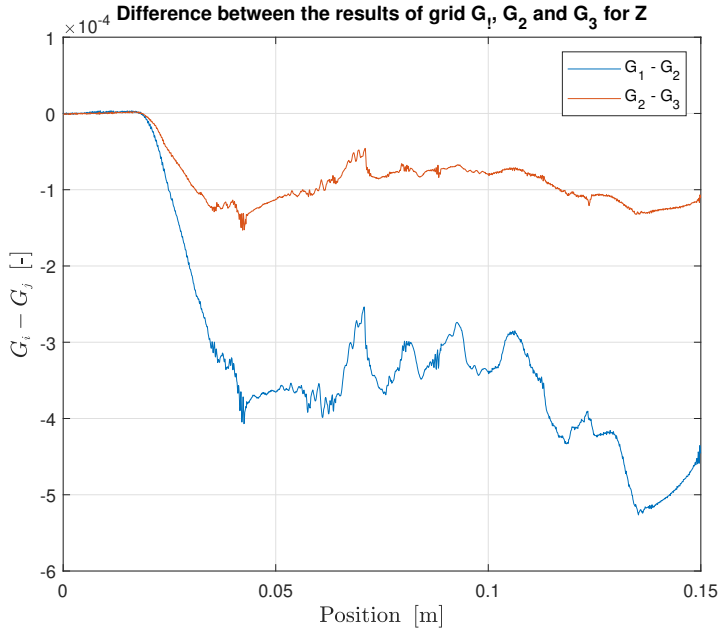

Figure 5.2: Differences of the Z results for grid G1, G2 and G3

Figure 5.3 shows the observed order of accuracy of t when Eq. (5.3) is applied on the Z results of grid GT1, GT2 and GT3.

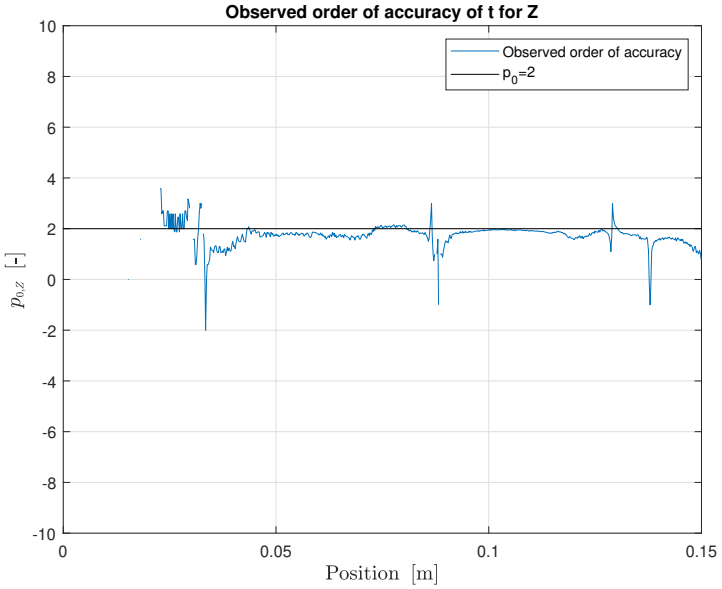

Figure 5.3: Observed order of accuracy of x for the mixture fraction

Figure 5.3 shows that the observed order of accuracy is around to 2 between x=0.05 m and

x=$0.15\,\mathrm{m}$. The Generalized Alpha time-scheme is a second order scheme, therefore the expected order of accuracy is 2, which is in line with the results. From x=$0\,\mathrm{m}$ to $0.04\,\mathrm{m}$ the observed order of accuracy is not a number. A possible reason for this behaviour is due to the finite file data precision as explained previously. This is observed in Figure 5.4, as the differences between the results approaches 0.

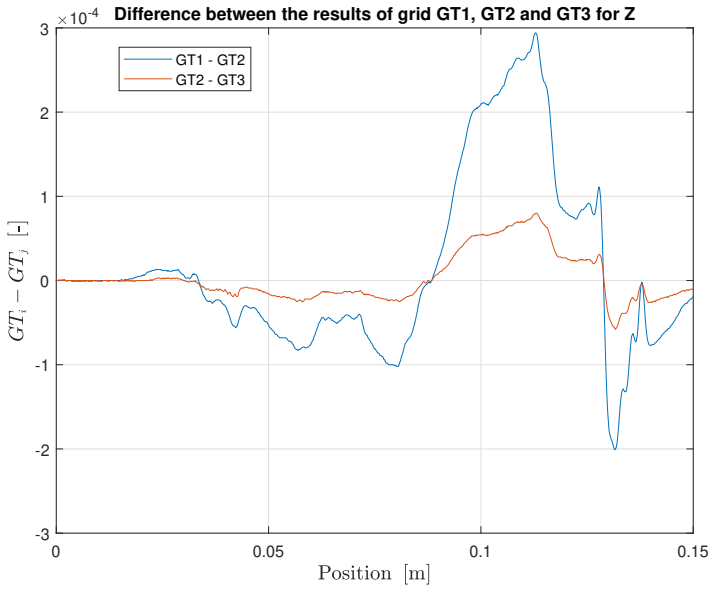

Figure 5.4: Differences of the Z results for grid GT1, GT2 and GT3

In summary, the observed order of accuracy for space and time are both equal to 2. Then the error can be estimated by taking the square of the step size in time or in space. Thus, when the reference case is taken as 800 elements and 6×10^4 time steps, the estimation of the error in x is 3.5156×10^{-8} and the estimation of the error in t is 2.5000×10^{-11}.

5.3 Performance of the simplified model in relation to the OpenFOAM model

The simplified model problem attempts to replicate the important characteristics of the mixing problem of a turbulent non-premixed combustion problem. The identified important variables are the mean and the RMS of u, Z and ϕ. Section 5.1. In this section the performance of the SMP model is investigated and compared to the OpenFOAM results as described in Section 5.1. In Figure 5.5 and Figure 5.6 the comparison can be found of respectively the mean and the RMS results of the OpenFOAM calculations and the reference case of the SMP test case.

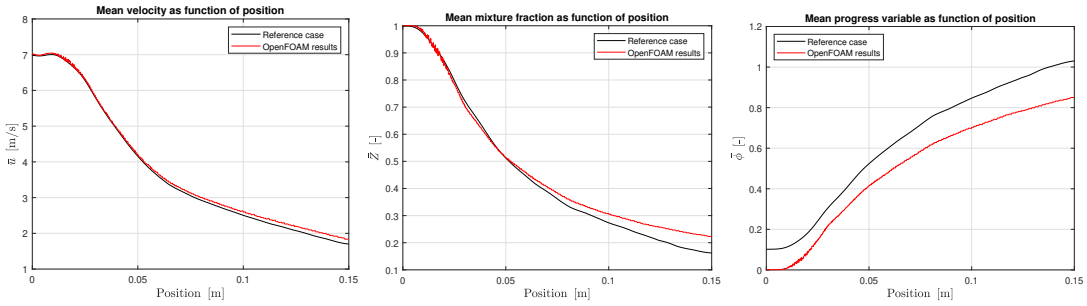

Figure 5.5: Comparison of the OpenFOAM mean results to the SMP test case mean results

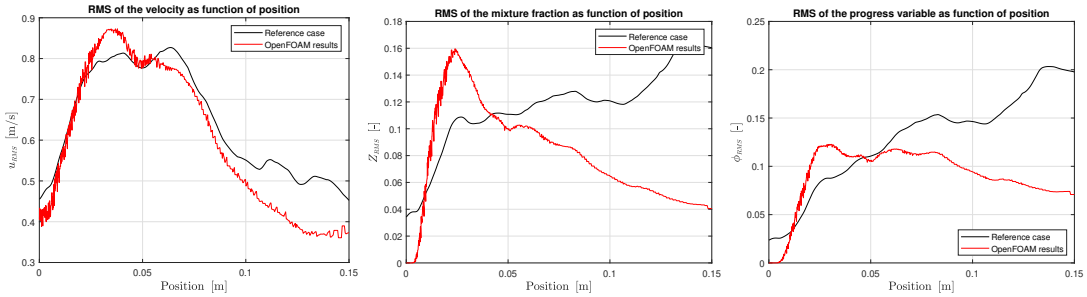

Figure 5.6: Comparison of the OpenFOAM RMS results to the SMP test case RMS results

Figure 5.5 shows that the mean results are comparable to each other. In Figure 5.6 there is a difference between the RMS results, especially for ϕ_{RMS} and Z_{RMS}.

In the list below the run time of the OpenFOAM simulations and Mex simulations are presented:

- OpenFOAM calculation (201 nodes in x-direction, 48 nodes in radial direction and 36 nodes in azimuthal direction): 2 days on 48 nodes
- VMM with implicit dynamic subscales: 1 hour for 100 elements, 1.5 hour for 200 elements and 2 hours for 300 elements all on 20 nodes
- Reference case (800 elements, no model): 2 hours on 20 nodes

All the simulations are run in parallel using 20 nodes. The OpenFOAM code is optimised to increase efficiency, whereas the Mex-code is optimised, but the SMP-code could be optimised in more detail.

When comparing the computational costs, it can be concluded that the computational costs for the SMP problem are lower compared to the OpenFOAM run. From the run time data and the comparison of the OpenFOAM results and the SMP results it is noted that the run time decreases dramatically when using the SMP model, but this decrease is at the expense of predicting a realistic RMS. Therefore the SMP model is not suitable to compare different models with experimental or DNS results.

Chapter 6

Coarse mesh SMP results

In order to investigate the potential of VMM for a turbulent non-premixed combustion problem, the SMP test case is used to compare several fine-scale models to a reference case. The following fine-scale models are considered in the SMP test case:

- No model
- Smagorinsky
- VMM with quasi-static subscales
- VMM with dynamic subscales (with implicit and explicit timescale)

The coarse-scale SMP test cases uses the mentioned fine-scale models and are run with different meshes and different definitions of τ and the obtained results are compared to the reference case. The setup of these simulations is described in Subsection 5.1.

6.1 Average results for different fine-scale models and τ_u

The average of the velocity u, mixture fraction Z and progress variable ϕ was computed using meshes of 100, 200 and 300 elements. The results are shown in Figure 6.1.

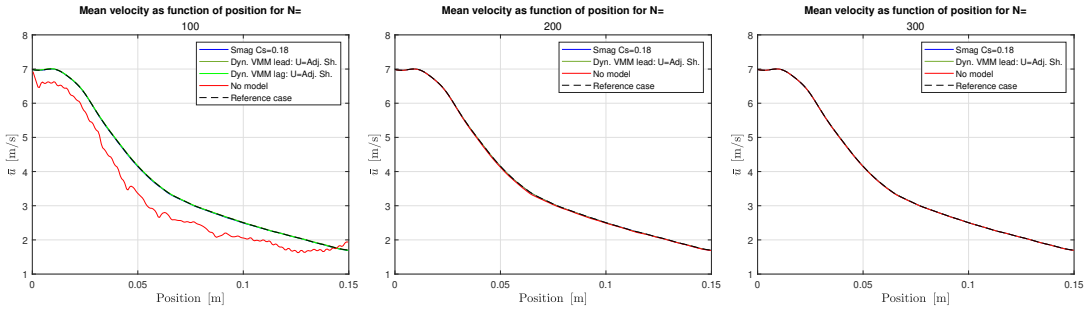

Figure 6.1: $\langle u \rangle$ results for N=100, N=200 and N=300

The calculated average of u for N=100, 200 and 300 elements are similar to the reference case when using Smagorinsky or VMM with implicit dynamic subscales as fine-scale model. When not using a fine-scale model the results are similar to the reference situation when N=200 and N=300 elements. The VMM models with dynamic subscales outperforms the Smagorinsky model.

VMM with explicit dynamic subscales are only shows stable results for 100 elements. VMM with quasi-static subscales is unstable for the selected number of elements.

The different definitions of τ_u are not presented in Figure 6.1, because the influence of τ_u on $\langle u \rangle$ are negligible on a plot. In Subsection 6.3 the influence of τ_u on the average results is analysed in detail.

The average of Z and ϕ for the selected number of elements are respectively presented in Figure 6.2 and Figure 6.3.

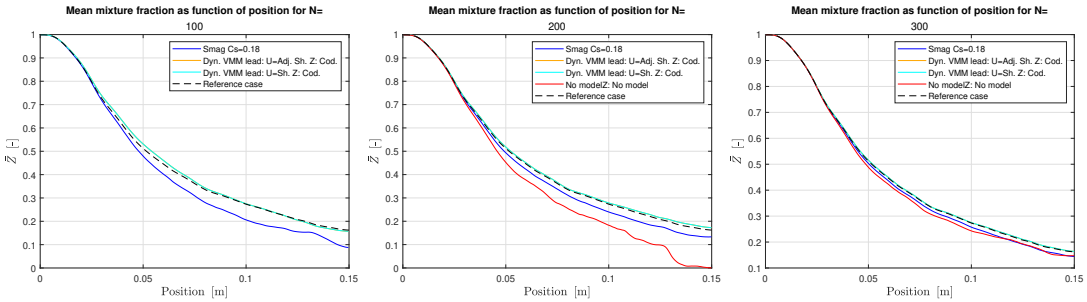

Figure 6.2: $\langle Z \rangle$ results for N=100, N=200 and N=300

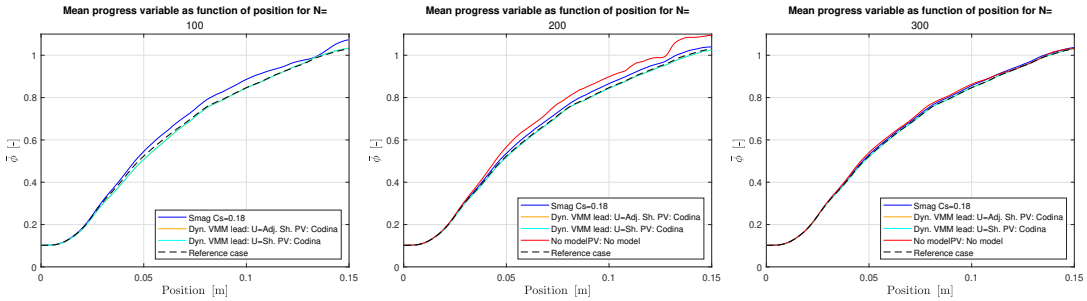

Figure 6.3: $\langle\phi\rangle$ results for N=100, N=200 and N=300

It is observed that the results for $\langle Z\rangle$ and $\langle\phi\rangle$ using VMM with implicit dynamic subscales are similar to the reference case for all the selected number of elements. For these variables, the results when using the Smagorinsky model differs with the reference case, but this difference decreases when the number of elements increases. When comparing the Smagorinsky model to the other VMM models, it is observed that the VMM model outperforms the Smagorinsky model. A possible reason could be that the Smagorinsky model always dissipates energy, whereas the VMM model does not show this effect.

VMM with explicit dynamic subscales are only stable when N=100 for $\langle Z\rangle$, for the other selected number of elements and for $\langle\phi\rangle$ the results are unstable. VMM with quasi-static subscales are unstable for all selected number of elements for $\langle\phi\rangle$ and $\langle Z\rangle$.

6.2 RMS results for different fine-scale models and τ_u

The RMS of u for the selected number of elements are presented in Figure 6.4.

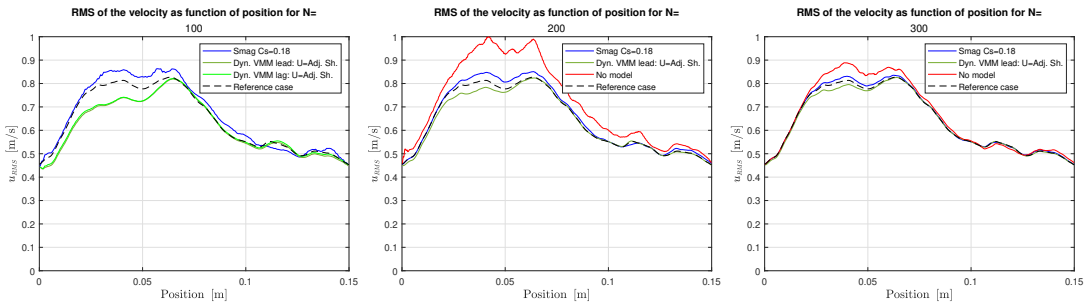

Figure 6.4: u_{RMS} results for N=100, N=200 and N=300

It is observed that for all selected elements the calculated RMS of u computed using VMM with implicit dynamic subscales matches the reference case well downstream of $x = 0.06$. In contrast the Smagorinsky model requires N=300 to produce similar results in this region. When looking at the region upstream from $x = 0.06$, it can be seen that the Smagorinsky model shows better results

compared to the different VMM models. A possible explanation for this effect is an oscillating forcing function of the Burgers equation in the first region. The RMS of u is shown in Figure 6.2. There is a sudden drop in the forcing function after the first element. This might explain

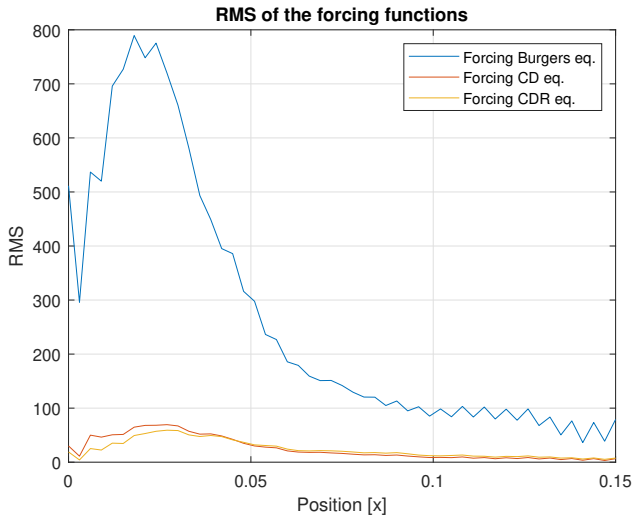

Figure 6.5: RMS of the forcing functions between t =0.3 s and t =0.45 s

the unexpected drop of u_{rms} after the first element for the VMM model results. This effect is not visible at the Smagorinsky results. As the Smagorinsky model always add dissipation to the system, this might lead to damp the effect of the oscillating forcing function.

The influence of using different τ_u definitions on u_{RMS} is negligible and hardly visible on a plot. The adjusted Shakib's definition shows slightly better results comparing to the original Shakib's definition.

The VMM model with explicit dynamic subscales assumption is only stable for 100 elements, whereas the quasi-static subscales assumption is unstable for all selected elements.

The RMS of Z and ϕ for the selected number of elements are presented in Figure 6.6 and Figure 6.7.

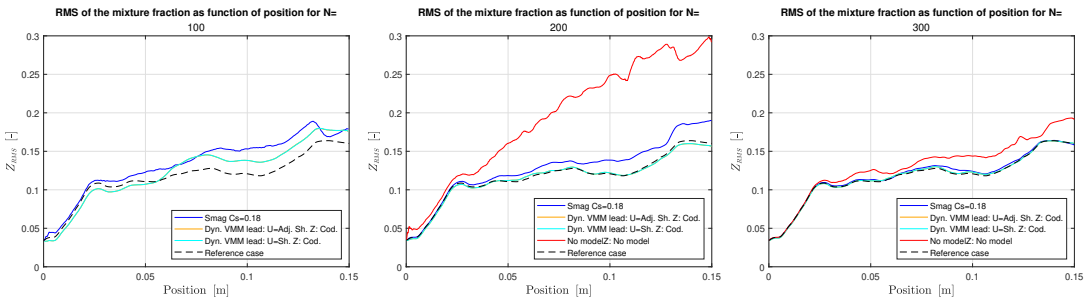

Figure 6.6: Z_{RMS} results for N=100, N=200 and N=300

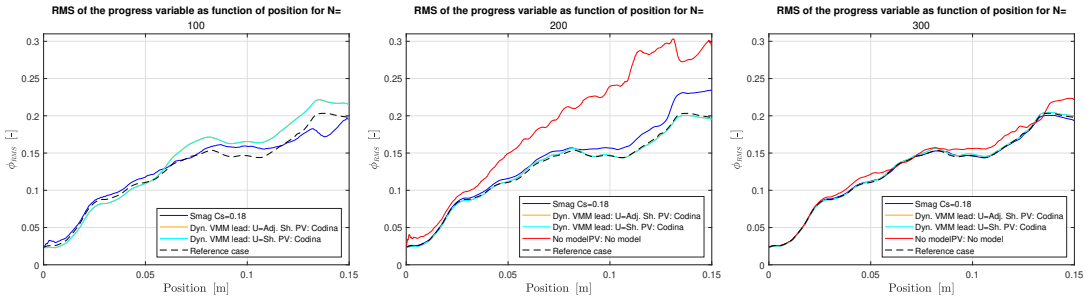

Figure 6.7: ϕ_{RMS} results for N=100, N=200 and N=300

The influence of τ_Z and τ_ϕ definitions on the RMS results is negligible compared to the influence of the fine-scale model. In Subsection 6.3 the influence of these parameters on the RMS results is analysed in more detail.

The results of Z_{RMS} and ϕ_{RMS} using VMM with implicit dynamic subscales match with the reference case for N=200 and N=300 elements. For these variables, the results when using the Smagorinsky model differs with the reference case, but the error decreases when the number of elements increases.

VMM with explicit dynamic subscales are stable when N=100 for Z_{RMS} and for ϕ_{RMS}. VMM with quasi-static subscales are unstable for all selected number of elements for Z_{RMS} and for ϕ_{RMS}.

In summary, the VMM model with dynamic subscales generally outperforms the Smagorinsky model.

6.3 Comparing τ results

The influence of the τ_u, τ_Z and τ_ϕ definitions could not be identified by presenting the results in several plots. The error between the SMP test case results and the reference case is thus presented in tables for 100, 200 and 300 elements. The quasi-static model is not included in the comparison, because for the selected number of elements, the model is unstable.

The results for $\langle u \rangle$ are shown in Table 6.1.

Only for 100 elements the explicit subscales model performs better than the VMM model with the implicit subscales assumption. For 300 elements Shakib's model performs slightly better than the adjusted Shakib's model [33]. The difference in error is maximal 1.4%. For 100 elements the performance is vise versa with a difference in error of 3.9%.

The τ definitions do not influence the stability of $\langle u \rangle$. The implicit subscale model is stable for all selected elements, whereas the explicit subscales model is only stable for 100 elements, regardless

Table 6.1: Error of $\langle u \rangle$ with respect to the reference case for several fine-scale models and selected τ_u

Fine-scale model	τ_u	Number of elements		
		300	200	100
VMM explicit subscales	Adj. Sh.	-	-	4.855×10^{-3}
VMM explicit subscales	Sh.	-	-	5.052×10^{-3}
VMM implicit subscales	Adj. Sh.	7.015×10^{-4}	1.526×10^{-3}	7.703×10^{-3}
VMM implicit subscales	Sh.	6.915×10^{-4}	1.526×10^{-3}	7.987×10^{-3}

of the selected τ definition.

The results for u_{RMS} are shown in Table 6.2.

Table 6.2: Error of u_{RMS} with respect to the reference case for several fine-scale models and selected τ_u

Fine-scale model	τ_u	Number of elements		
		300	200	100
VMM explicit subscales	Adj. Sh.	-	-	3.882×10^{-2}
VMM explicit subscales	Sh.	-	-	3.871×10^{-2}
VMM implicit subscales	Adj. Sh.	8.751×10^{-3}	1.524×10^{-2}	4.171×10^{-2}
VMM implicit subscales	Sh.	8.776×10^{-3}	1.516×10^{-2}	4.165×10^{-2}

The results using Shakib's model and the adjusted Shakib's model are similar for u_{RMS}.

The τ definitions do not influence the stability of u_{RMS}. The implicit subscale model is stable for all selected elements, whereas the explicit subscales model is only stable for 100 elements, regardless of the selected τ definition.

For the investigation of the error of Z and ϕ, only the error of the mean values are presented as the error of the mean value and RMS value are similar to each other.

The results for $\langle \phi \rangle$ are shown in Table 6.3.

The application of adjusted Shakib's model for τ_u yields better results for 200 and 300 elements. The maximum difference in error is 8.6% when comparing the different τ_u results for 300 elements. When comparing the different τ_ϕ models, it is observed that Franca and Valentina's model performs worst and Codina's model performs best. The difference in error is maximum 3.6%, which is achieved for 300 elements and using the adjusted Shakib's model forτ_u. In Appendix B.1, the results of all τ_ϕ runs are presented.

The results for $\langle Z \rangle$ are shown in Table 6.4.

Table 6.3: Error of $\langle\phi\rangle$ with respect to the reference case for several fine-scale models and for a selection of τ_ϕ

Fine-scale model	τ_u	τ_ϕ	Number of elements		
			300	200	100
VMM implicit subscales	Adj. Sh.	Cod.	1.489×10^{-3}	3.778×10^{-3}	7.482×10^{-3}
VMM implicit subscales	Adj. Sh.	F&V	1.544×10^{-3}	3.820×10^{-3}	7.504×10^{-3}
VMM implicit subscales	Sh.	Cod.	1.627×10^{-3}	3.879×10^{-3}	7.420×10^{-3}
VMM implicit subscales	Sh.	F&V	1.684×10^{-3}	3.934×10^{-3}	7.450×10^{-3}

Table 6.4: Error of $\langle Z\rangle$ with respect to the reference case for several fine-scale models and for a selection of τ_Z

Fine-scale model	τ_u	τ_Z	Number of elements		
			300	200	100
VMM implicit subscales	Adj. Sh.	F&V	2.324×10^{-3}	6.142×10^{-3}	9.468×10^{-3}
VMM implicit subscales	Adj. Sh.	st. des.	2.188×10^{-3}	5.983×10^{-3}	9.284×10^{-3}
VMM implicit subscales	Sh.	F&V	2.526×10^{-3}	6.273×10^{-3}	9.417×10^{-3}
VMM implicit subscales	Sh.	st. des.	2.394×10^{-3}	6.104×10^{-3}	9.222×10^{-3}

The application of adjusted Shakib's model for τ_u yields better results for 200 and 300 elements. The maximum difference in error is 8.6%. When comparing the different τ_Z models, it is observed that Franca and Valentina's model performs worst and the standard design model performs best. The difference in error is maximum 5.9%, which is achieved for 300 elements and using the adjusted Shakib's model for τ_u. A possible reason for this behaviour is that the coefficients of the adjusted Shakib's model are optimized for a channel flow simulation using the Burgers equation.In Appendix B.1, the results of all τ_Z runs are presented.

As indicated previously the VMM quasi-static subscale model is unstable for u, Z and ϕ. This could be solved by decreasing the time-step of the SMP test case. In the next subsection the influence of the timestep on the various VMM models is investigated.

6.4 Sensitive analysis time step

In this section the influence of the time step related to the performance of the VMM quasi static and dynamic subscale model is investigated.

For the VMM quasi-static subscale model test cases, the following time steps are considered: $2.5 \times 10^{-6}\,\mathrm{s}$, $1.25 \times 10^{-6}\,\mathrm{s}$, $6.25 \times 10^{-7}\,\mathrm{s}$, $3.125 \times 10^{-7}\,\mathrm{s}$ and $1.5625 \times 10^{-7}\,\mathrm{s}$. For all time steps the model is unstable. A possible reason for this behaviour is that the SMP test case is based on

a non-premixed combustion problem, which is a transient problem. Also combustion occur at the smallest timescales. As indicated by Codina et al. [9], implementing a quasi-static assumption for a transient problem might lead to errors, which is a possible source of error for the considered behaviour.

For the analysis on the performance of the dynamic VMM models on the time step, a time step of $2.5 \times 10^{-6}\,\mathrm{s}$ is considered.

The results of the error compared to the reference case for the mean values are presented in Table 6.5. The VMM model with the explicit subscales assumption is still unstable or shows unrealistic values for 200 and 300 elements. Therefore only the results of 100 elements are presented in the tables.

Table 6.5: Error of the mean results for different time steps

VMM model	Mean results					
	u		ϕ		Z	
	$2.5 \times 10^{-6}\,\mathrm{s}$	$5 \times 10^{-6}\,\mathrm{s}$	$2.5 \times 10^{-6}\,\mathrm{s}$	$5 \times 10^{-6}\,\mathrm{s}$	$2.5 \times 10^{-6}\,\mathrm{s}$	$5 \times 10^{-6}\,\mathrm{s}$
explicit subsc	5.470×10^{-3}	4.86×10^{-3}	7.527×10^{-3}	-	9.406×10^{-3}	-
implicit subsc	4.060×10^{-3}	7.70×10^{-3}	7.597×10^{-3}	7.341×10^{-3}	1.064×10^{-2}	9.222×10^{-3}

The results of the error compared to the reference case for the RMS values are presented in Table 6.6.

Table 6.6: Error of the RMS results for different time steps

VMM model	Mean results					
	u		ϕ		Z	
	$2.5 \times 10^{-6}\,\mathrm{s}$	$5 \times 10^{-6}\,\mathrm{s}$	$2.5 \times 10^{-6}\,\mathrm{s}$	$5 \times 10^{-6}\,\mathrm{s}$	$2.5 \times 10^{-6}\,\mathrm{s}$	$5 \times 10^{-6}\,\mathrm{s}$
explicit subsc.	4.202×10^{-2}	3.88×10^{-2}	1.478×10^{-2}	-	1.339×10^{-2}	-
implicit subsc	3.290×10^{-2}	4.17×10^{-2}	1.431×10^{-2}	1.438×10^{-2}	1.517×10^{-2}	1.320×10^{-2}

As the influence of τ is not taken into account, only the best performing τ are analysed, which is the adjusted Shakib's model for τ_u, the standard design for τ_Z and Shakib's for τ_ϕ.

The time step is not further decreased, because the duration of 1 run with a time step of $2.5 \times 10^{-6}\,\mathrm{s}$ takes approximately 1.75 hrs on 20 cores using the optimised code. But the presented results gives some insight into the performance of the various VMM models in relation to the time step in relation to. From Table 6.5 and Table 6.6, it is observed that decreasing the time step leads to a stable VMM model with the explicit subscales assumption for u, Z and ϕ. For a time step of $2.5 \times 10^{-6}\,\mathrm{s}$, the VMM model with the implicit subscales assumption outperforms the VMM model with the explicit subscales assumption for u. The difference is 25.8% and 21.7% for respectively $\langle u \rangle$ and u_{RMS}. For $\langle \phi \rangle$, ϕ_{RMS} and $\langle Z \rangle$ the results are comparable to each other. However, the VMM model with the explicit subscales assumption for Z_{RMS} outperforms the VMM model with

the implicit subscales assumption, the difference between the different dynamic models is 11.7%.

A possible reason for the overall better accuracy of the VMM model with the implicit subscales assumption is the choice of the time march scheme. For this SMP test case the Generalized alpha time march scheme is chosen. In summary, due to the chosen coefficients the Generalized alpha time scheme in the SMP model calculates the variables at a different time. For example, if $t_{n-1} - t_n$ is $5 \times 10^{-6}\,\mathrm{s}$, the Generalized alpha time march scheme determines the velocity, mixture fraction and progress variable at $0.333 \times 10^{-6}\,\mathrm{s}$. As this value is closer to $5 \times 10^{-6}\,\mathrm{s}$ compared to $0\,\mathrm{s}$, the computed time derivatives at time $0.333 \times 10^{-6}\,\mathrm{s}$ show more resemblance with the estimated time derivatives used in the VMM model with the implicit subscales assumption compared to the estimated time derivatives in the VMM model with the explicit subscales assumption. This is a possible reason for a better accuracy of the VMM model with the implicit subscales assumption model compared to the other VMM fine-scale models.

When analysing the influence of the time step itself on the results, it is observed that the error of the mean and RMS results of u improves when decreasing the time step. The largest improvement can be seen for $\langle u \rangle$, where the difference of the error is 47.7%. The performance of the determination of ϕ does not improve significantly when decreasing the time step. And the determination of Z becomes worse when decreasing the time step.

When looking at the stability of the results, it can be seen that the simulations which use the explicit subscale assumption return stable solutions, whereas the simulations with the explicit subscale assumption is only stable when decreasing the time step. A possible reason for this effect is that the explicit subscale assumption can be compared to an explicit method, whereas the implicit subscale assumption to an implicit method. The backward Euler scheme (an implicit method) is generally unconditionally stable, whereas the forward Euler scheme (an explicit method) is usually conditionally stable [5].

Chapter 7

Conclusions and recommendations

A simplified model problem has been developed which has the important aspects of turbulent non-premixed combustion for comparing numerical methods. An important reason to construct the simplified model problem is that fully 3D results are expensive to run and more importantly the results are difficult to interpret due to their complexity. Because non-premixed combustion is a complex process, the proposed simplified model problem reduces the complexity of the problem yet includes many of its important characteristics.

Using the simplified model problem, a framework based on the VMM formulation is proposed for non-premixed combustion computations and its potential is investigated by comparing the results using several definitions of τ, which describes the fine-scale variables. These results are compared with the results using a Smagorinsky model to a reference case.

7.1 Conclusions

The answers to the research questions presented in Section 1.3 are shown below.

RQ 1: What are the differences between the simplified model and a full 3D non-premixed combustion model? The mean results of the relevant variables are comparable to the results of the considered full 3D turbulent non-premixed combustion problem. However the RMS results of the relevant variables deviates from each other, especially for ϕ_{RMS} and Z_{RMS}. As the SMP model has a forcing term which includes the 12 lowest wave numbers, it can be concluded that the RMS is highly dependent on the higher wave numbers.

The computational costs for the SMP problem are much lower than that of the OpenFOAM runs. However this decrease is at the expense of predicting a realistic RMS. Therefore the SMP model is in this sense not suitable for comparison with experimental or DNS results.

RQ 2: Is the current definition of τ sufficient for the simplified model problem? When investigating the original τ definitions, it was demonstrated that these discretisation are not Galilean invariant. To fix this discrepancy, all τ definitions were adjusted to be Galilean invariant by introducing a shift with a reference velocity.

RQ 3: How do the methods compare in their ability to reproduce the statistics of the relevant variables? For the mean value of the relevant variables the VMM model with the implicit dynamic subscale assumption outperforms the other VMM models and the Smagorinsky model for all variables. Even for a coarse mesh the mean results of the VMM model with the implicit dynamic subscale assumption matches the reference case.

For the RMS values the VMM model with the implicit dynamic subscale assumption outperforms the other VMM models and the Smagorinsky model for the mixture fraction and the progress variable. When the mesh is refined, the RMS results of the VMM model with the implicit dynamic subscale assumption matches with the results of the reference case faster than the Smagorinsky model. When determining the RMS results of u, the VMM model shows better results compared the the Smagorinsky model only in the second part of the domain. The effect of a heavy oscillating forcing function of the Burgers equation in the first part of the domain may be a factor in this discrepancy.

RQ 4: Which of the τ definitions for the flow field, reaction terms and for a passive scalar are most effective? The adjusted Shakib's model [33] for τ_u yields better results compared to Shakib's model, especially for a fine mesh. A possible reason for this behaviour is that the coefficients of the adjusted Shakib's model are optimized for a channel flow simulation using the Burgers equation.

The difference in effectiveness of the considered τ_Z and τ_ϕ definitions are minimal. When comparing the different τ_ϕ models, it can be seen that Franca and Valentina's [19] model performs worst while Codina's [7] model performs best. The difference in error is maximum 3.6%. When comparing the different τ_Z models, it can be seen that Franca and Valentina's model performs worst and the standard design model performs best. The difference in error is maximum 5.9%.

RQ 5: What is the performance of the different assumptions for the subscales on the results? The SMP test cases using the VMM model with quasi-static subscale assumption remain unstable for the lowest considered time step of $1.5625\times10^{-7}\,\mathrm{s}$. A possible reason for this behaviour is that the SMP test case is based on a non-premixed combustion problem, in which combustion occurs at the smallest timescales. As indicated by Codina et al. [9], implementing a quasi-static assumption for a strongly transient problem might lead to errors, which is a possible source of the unstable behaviour of the quasi-static subscales assumption.

In contrast the VMM model with dynamic subscales performed well. The dynamic subscale model with the implicit dynamic subscales assumption generally perform better than that with the explicit dynamic subscale assumption, especially for stability.

7.2 Recommendation

The research revealed that the dynamic VMM formulation with the implicit dynamic subscales assumption outperforms the Smagorinsky model using the simplified model problem. Therefore potentially the VMM formulation of a 3D turbulent non-premixed combustion problem could outperform the standard sub-grid models. On this basis, the following recommendations are made:

Conduct 3D turbulent non-premixed simulation runs Future research should implement VMM for a full 3D turbulent non-premixed combustion problem to investigate the potential of VMM related to the performance of predicting the relevant variables. First it is advised to focus on the mixing problem, because VMM has the potential to improve the prediction of the outcome of this problem. Next is to incorporate the flame structure models into the problem and to compare full 3D LES simulations and to experimental or DNS results .

Use a non-diagonal τ In this work a diagonal τ is used, which means that the fine-scale u', Z' and ϕ' is only dependent on its residual, either $\mathcal{L}\overline{u} - f_B$, $\mathcal{L}\overline{Z} - f_{CD}$ or $\mathcal{L}\overline{\phi} - f_{CDR}$. As a consequence, τ can be set separately for the Burgers, CD and CDR equation. Because combustion occurs at the smallest scales, interaction between the flow variables could take place at the fine-scales. By incorporating a non-diagonal τ, an attempt could be made to model interactions at the fine-scale levels.

The choice of the reference velocity in the adjust τ definition Another interesting feature which can be incorporated is the choice of u_{ref} in order to transform τ to a Galilean invariant term. In this work, a simplified method is chosen. It can be useful to explore the potential of a varying u_{ref}, which might improve the prediction of the RMS.

Bibliography

[1] N.A. Adams and S. Hickel. Implicit large-eddy simulation: Theory and application. In *Advances in Turbulence XII: Proceedings of the 12th EUROMECH European Turbulence Conference, September 7-10, 2009, Marburg, Germany*, pages 743–750. Springer, 2009.

[2] Y. Bazilevs, V.M. Calo, J.A. Cottrell, T.J.R. Hughes, A. Reali, and G. Scovazzi. Variational multiscale residual-based turbulence modeling for large eddy simulation of incompressible flows. *Computer Methods in Applied Mechanics and Engineering*, 197(1):173–201, 2007.

[3] K.N.C. Bray. The challenge of turbulent combustion. In *Symposium (International) on Combustion*, volume 26, pages 1–26, 1996.

[4] J.M. Burgers. A mathematical model illustrating the theory of turbulence. In *Advances in applied mechanics*, volume 1, pages 171–199. Elsevier, 1948.

[5] J.C. Butcher. *Numerical methods for ordinary differential equations*. John Wiley & Sons, 2016.

[6] V.M. Calo. *Residual-based multiscale turbulence modeling: finite volume simulations of bypass transition*. PhD thesis, Stanford University, 2004.

[7] R. Codina. Comparison of some finite element methods for solving the diffusion-convection-reaction equation. *Computer Methods in Applied Mechanics and Engineering*, 156(1):185–210, 1998.

[8] R. Codina. Stabilization of incompressibility and convection through orthogonal sub-scales in finite element methods. *Computer methods in applied mechanics and engineering*, 190 (13-14):1579–1599, 2000.

[9] R. Codina, J. Principe, O. Guasch, and S. Badia. Time dependent subscales in the stabilized finite element approximation of incompressible flow problems. *Computer Methods in Applied Mechanics and Engineering*, 196(21-24):2413–2430, 2007.

[10] S. Collis. Monitoring unresolved scales in multiscale turbulence modeling. *Physics of Fluids*, 13:1800, 2001.

[11] S. De, Avinash K. Agarwal, S. Chaudhuri, and S. Sen. *Modeling and simulation of turbulent combustion*. Springer, 2018.

[12] A. Ern and V. Giovangigli. *Multicomponent transport algorithms*, volume 24. Springer Science & Business Media, 1994.

[13] G. Esposito and H.K. Chelliah. Skeletal reaction models based on principal component analysis: Application to ethylene–air ignition, propagation, and extinction phenomena. *Combustion and Flame*, 158(3):477–489, 2011.

[14] L.P. Franca and F. Valentin. On an improved unusual stabilized finite element method for the advective–reactive–diffusive equation. *Computer Methods in Applied Mechanics and Engineering*, 190(13):1785–1800, 2000.

[15] V. Gravemeier. *The variational multiscale method for laminar and turbulent incompressible flow*. Universität Stuttgart, 2003.

[16] V. Gravemeier. The variational multiscale method for laminar and turbulent flow. *Archives of Computational Methods in Engineering*, 13(2):249–324, 2006.

[17] V. Gravemeier and W.A. Wall. Variational multiscale methods for premixed combustion based on a progress-variable approach. *Combustion and Flame*, 158(6):1160–1170, 2011.

[18] G. Hauke. Simple stabilizing matrices for the computation of compressible flows in primitive variables. *Computer methods in applied mechanics and engineering*, 190(51-52):6881–6893, 2001.

[19] G. Hauke and A. Garcia-Olivares. Variational subgrid scale formulations for the advection-diffusion-reaction equation. *Computational Methods Applied Mechanical Engineering*, 190: 6847–6865, 2001.

[20] E. Hopf. The partial differential equation ut+ uux= μxx. *Communications on Pure and Applied mathematics*, 3(3):201–230, 1950.

[21] T. Hughes and G. Sangalli. Variational multiscale analysis: the fine-scale green's function, projection, optimization, localization, and stabilized methods. *SIAM Journal on Numerical Analysis*, 45(2):539–557, 2007.

[22] T.J.R. Hughes. Multiscale phenomena: Green's functions, the dirichlet-to-neumann formulation, subgrid scale models, bubbles and the origins of stabilized methods. *Computer methods in applied mechanics and engineering*, 127(1):387–401, 1995.

[23] T.J.R. Hughes and M. Mallet. A new finite element formulation for computational fluid dynamics: Iv. a discontinuity-capturing operator for multidimensional advective-diffusive systems. *Computer methods in applied mechanics and engineering*, 58(3):329–336, 1986.

[24] T.J.R. Hughes, G.R. Feijóo, L. Mazzei, and J. Quincy. The variational multiscale method—a paradigm for computational mechanics. *Computer methods in applied mechanics and engineering*, 166(1):3–24, 1998.

[25] T.J.R. Hughes, L. Mazzei, and K.E. Jansen. Large eddy simulation and the variational multiscale method. *Computing and Visualization in Science*, 3(1-2):47–59, 2000.

[26] T.J.R. Hughes, G. Scovazzi, and T.E. Tezduyar. Stabilized methods for compressible flows. *Journal of Scientific Computing*, 43(3):343–368, 2010.

[27] B.B. Ilyushin and D.V. Krasinsky. Large eddy simulation of the turbulent round jet dynamics. *Thermophysics and Aeromechanics*, 13:43–54, 2006.

[28] M. Karaca, I. Fedioun, and N. Lardjane. High-speed turbulent mixing and combustion: Miles vs physical les. In *TSFP DIGITAL LIBRARY ONLINE*. Begel House Inc., 2011.

[29] M Karaca, N Lardjane, and I Fedioun. Implicit large eddy simulation of high-speed non-reacting and reacting air/h2 jets with a 5th order weno scheme. *Computers & Fluids*, 62: 25–44, 2012.

[30] L.A. Klaessen. *Modeling of MILD combustion and the influence of sub-grid scale models*. PhD thesis, Delft University of Technology, 2012.

[31] V.R. Kuznetsov. Influence of turbulence on the formation of high nonequilibrium concentrations of atoms and free radicals in diffusion flames. *Fluid Dynamics*, 17(6):815–820, 1982.

[32] C.K. Law. Combustion at a crossroads: Status and prospects. *Proceedings of the Combustion Institute*, 31(1):1–29, 2007.

[33] L.C. Navarro Hernandez. *Design of residual-based unresolved-scale models using time-averaged data*. PhD thesis, Delft University of Technology, 2015.

[34] F.T. Nieuwstadt and J.A. Steketee. *Selected papers of JM Burgers*. Springer Science & Business Media, 2012.

[35] P. Pepiot and H. Pitsch. Systematic reduction of large chemical mechanisms. In *4th Joint Meeting of the US Sections of the Combustion Institute*, volume 2123, page 2005. Drexel University Pittsburgh, PA, USA, 2005.

[36] N. Peters. *Turbulent combustion*. Cambridge University Press, 2000.

[37] N. Peters. Local quenching of diffusion flamelets and non-premixed turbulent combustion. In *Paper WSS 80-4*. Spring Meeting, Irvine, CA, 1980.

[38] N. Peters. Multiscale combustion and turbulence. *Proceedings of the Combustion Institute*, 32(1):1–25, 2009.

[39] C.D. Pierce and P. Moin. *Progress-variable approach for large-eddy simulation of turbulent combustion*. PhD thesis, Citeseer, 2001.

[40] C.D. Pierce and P. Moin. Progress-variable approach for large-eddy simulation of non-premixed turbulent combustion. *Journal of Fluid Mechanics*, 504:73–97, 2004.

[41] T. Poinsot and D. Veynante. *Theoretical and Numerical Combustion*. Edwards, second edition, 2005.

[42] S.B. Pope. Computationally efficient implementation of combustion chemistry using in situ adaptive tabulation. *Combustion Theory and Modelling*, 1(1):41–63, 1997.

[43] S.B. Pope. *Turbulent flows*. Cambridge University Press, 2000.

[44] Stephen B Pope. Small scales, many species and the manifold challenges of turbulent combustion. *Proceedings of the Combustion Institute*, 34, 2012.

[45] P.J. Roache. Code verification by the method of manufactured solutions. *Journal of Fluids Engineering*, 124(1):4–10, 2002.

[46] P. Sagaut. *Large eddy simulation for incompressible flows*. Springer, 2006.

[47] G.. Scovazzi. *Multiscale methods in science and engineering*. PhD thesis, Stanford University, 2004.

[48] F. Shakib, T.J.R. Hughes, and Z. Johan. A new finite element formulation for computational fluid dynamics: X. the compressible euler and navier-stokes equations. *Computer Methods in Applied Mechanics and Engineering*, 89(1):141–219, 1991.

[49] G.P. Smith, D.M. Golden, M. Frenklach, N.W. Moriarty, B. Eiteneer, M. Goldenberg, C.T. Bowman, R.K. Hanson, S. Song, W.C. Gardiner, Jr., Lissianski V.V., and Z. Qin. Gri-mech 3.0, july 2012. URL http://www.me.berkeley.edu/gri_mech/.

[50] C.J. Sung, C.K. Law, and J-Y Chen. An augmented reduced mechanism for methane oxidation with comprehensive global parametric validation. In *Symposium (International) on Combustion*, volume 27, pages 295–304. Elsevier, 1998.

[51] F. Wang, P. Li, G. Wang, and J. Mi. Moderate and intense low-oxygen dilution (mild) combustion of liquid fuels: A review. *Energy & Fuels*, 36(15):8026–8053, 2022.

[52] Z. Warhaft. Passive scalars in turbulent flows. *Annual Review of Fluid Mechanics*, 32(1): 203–240, 2000.

[53] F.A. Williams. *Combustion Theory*. Princeton University, 1985.

[54] S. Zhao. *Explicit and implicit large eddy simulation of turbulent combustion with multi-scale forcing*. PhD thesis, Université d'Orléans, 2016.

[55] S. Zhao, N Lardjane, and I. Fedioun. Comparison of improved finite-difference weno schemes for the implicit large eddy simulation of turbulent non-reacting and reacting high-speed shear flows. *Computers & Fluids*, 95:74–87, 2014.

Appendix A

Theory and modelling of non-premixed combustion

Non-premixed combustion occurs when fuel and oxidizer are in a separated stream and are mixed together as such that a combustible mixture is formed. When the combustible mixture is ignited, rapid chemical reaction at the interface of the fuel and oxidizer stream occurs in a thin region. Reactants and the most important product, heat are formed which can be used to generate power. Combustion in a fluid flow is a complex process, because combustion affects fluid flow and visa versa. Due to the added heat physical properties, such as viscosity, changes, which affects fluid flow. For non-premixed combustion, mixing is an important physical phenomenon, and mixing is caused by the fluid flow. In comparison with premixed combustion, where fuel and oxidizer are already mixed at a molecular level, mixing is not relevant in this process.

In order to improve power generation and to decrease pollutants, the characteristics and the physical processes of non-premixed combustion must be understood. This chapter shows the theoretical background of non-premixed turbulent combustion to gain insight in the physical mechanisms and the imposed assumptions when modelling combustion. With this knowledge, the most important characteristics of non-premixed combustion can be extracted, which is the origin of the simplified combustion model problem. The chapter exists of two section. First section shows the theoretical background of laminar non-premixed combustion and shows the current methodology of modeling laminar non-premixed combustion. The second section shows the influence of turbulence on non-premixed combustion. Because turbulence alters the fluid flow and therefore alters mixing, an additional process is introduced in non-premixed combustion. In this section also several methods to model turbulent non-premixed combustion are presented.

A.1 Laminar non-premixed combustion

In order to focus on the important aspects of non-premixed combustion, this section provides the theoretical background and methodology of modelling laminar non-premixed combustion. First subsection provides the starting point of combustion, namely the governing equations of compressible reacting flow. Second section explains the chemistry kinetics involved in combustion, and to be more precise, in the chemical reactions of hydrocarbons. In the third section, the general aspects of laminar non-premixed flames are presented, including several assumptions which are needed to split a laminar non-premixed problem into a laminar mixing problem and a laminar flame structure problem. The latter determines the chemical properties. Both problems are explained in the fourth and fifth subsection respectively.

A.1.1 Governing equations of compressible reacting flow

Non-premixed combustion involves numerous different species reacting through multiple chemical reactions. This means that the flow properties are dependent of the mixture composition and therefore the continuity equation, Navier-Stokes equations and the energy equation require some adjustments to characterize the flow.

Consider a mixture which exists of N different species, the mass fractions Y_k of species k are defined as:

$$Y_k = \frac{m_k}{m} \tag{A.1}$$

where m_k is the mass of species k in a fixed volume V and m is the total mass in this volume. The mole fraction X_k of species k in the considered mixture is defined as:

$$X_k = \frac{C_k}{C} \tag{A.2}$$

where C_k is the number of moles of species k in a fixed volume V and m is the total mass in this volume and C is the number of moles for all species in the same volume. Both non-dimensional quantities are equal to 1 if it's summed over all species. In a mixture, the mass fraction or mole fraction relates the behaviour of the quantity of the individual species and the quantity of the mixture. For example, the density of the mixture is related to the density of each individual species by the mass fraction:

$$\rho_k = \sum_{k=1}^{N} Y_k \rho \tag{A.3}$$

where ρ_k is the density of species k and ρ is the density of the mixture. Another example is the relation of the velocity of the mixture and the velocity of the individual components of the mixture:

$$u_{k,i} = Y_k u_i \tag{A.4}$$

where $u_{k,i}$ is the velocity of species k in the mixture and u_i is the velocity of the mixture. A final example shows the relation of the total pressure and partial pressure of the individual components of the mixture:

$$p_k = X_k p \tag{A.5}$$

where p_k is the partial pressure of species k in the mixture and p is the pressure of the mixture. When summing the individual components of a quantity, the result is the total quantity corresponding to the mixture.

In a fluid flow problem with chemical reactions, mechanical and thermal variables are involved. In addition, also information about each species needs to be determined. For the derivation of the conservation equations for laminar non-premixed combustion, several variables needs to be solved. In this thesis, these variables which are related to the fluid flow are:

- Density ρ
- Three dimensional velocity u_i in i-direction, in which $i = 1, 2, 3$
- Energy, enthalpy or temperature. The choice depends on the problem which needs to be solved
- Mass fractions Y_k of the N species involved in the mixture

When looking at the listed variables, it can be seen that $N + 5$ variables needs to be solved when dealing with a compressible reacting flow. Therefore $N + 5$ equations are needed to solve the important variables of a laminar reaction fluid flow problem. The starting point of the derivation of the relevant conservation equations for laminar non-premixed combustion is compressible flow. This means that the momentum equation and energy equation is a coupled system. All presented equations are written in the index notation, which implies summation over the repeated indices, except for the index which indicate the different species.

Continuity and momentum equation

The continuity equation for compressible flow is given by:

$$\frac{\partial \rho}{\partial t} + \frac{\partial \rho u_i}{\partial x_i} = 0 \tag{A.6}$$

The momentum equations (or Navier-Stokes equations) for a compressible mixture is:

$$\frac{\partial \rho u_j}{\partial t} + \frac{\partial}{\partial x_i}\left(\rho u_i u_j\right) = \frac{\partial \sigma_{ij}}{\partial x_i} + \rho \sum_{k=1}^{N} Y_k f_{k,j} \tag{A.7}$$

where $f_{k,j}$ is the body force exerted on species k in the fluid and σ_{ij} is the stress tensor. Combining Eq.(A.6) and Eq.(A.7) gives:

$$\rho \frac{\partial u_j}{\partial t} + \rho u_i \frac{\partial u_j}{\partial x_i} = \rho \frac{D u_j}{D t} = \frac{\partial \sigma_{ij}}{\partial x_i} + \rho \sum_{k=1}^{N} Y_k f_{k,j} \tag{A.8}$$

where $\frac{D}{Dt} = \frac{\partial}{\partial t} + u_i \frac{\partial}{\partial x_i}$ is the material derivative. For a Newtonian fluid, the stress tensor can be written as:

$$\sigma_{ij} = -p\delta_{ij} + \left(\lambda + \frac{2}{3}\mu\right)\frac{\partial u_i}{\partial x_i}\delta_{ij} + \mu\left(\frac{\partial u_i}{\partial x_j} + \frac{\partial u_j}{\partial x_i} - \frac{2}{3}\frac{\partial u_i}{\partial x_i}\right) \tag{A.9}$$

where μ is the dynamic viscosity coefficient, λ is the coefficient of bulk viscosity and δ_{ij} is the Kronecker delta, which is defined as:

$$\delta_{ij} = \begin{cases} 1 & \text{if } i = j \\ 0 & \text{if } i \neq j \end{cases} \tag{A.10}$$

The term $\lambda + \frac{2}{3}\mu$ is also known as the second viscosity ζ. This term is important when dealing with processes such as sound absorption. When neglecting this term., combining Eq (A.9) with Eq.(A.8) gives:

$$\rho\frac{Du_j}{Dt} = -\frac{\partial p}{\partial x_j} + \frac{\partial}{\partial x_j}\left(\mu\left(\frac{\partial u_i}{\partial x_j} + \frac{\partial u_j}{\partial x_i} - \frac{2}{3}\frac{\partial u_i}{\partial x_i}\right)\right) + \rho\sum_{k=1}^{N} Y_k f_{k,j} \tag{A.11}$$

For the momentum equation, the pressure is needed. The pressure can be obtained by using the equation of state, which relates the pressure, temperature and the density. It reads:

$$p = \frac{\rho R_u T}{W} \tag{A.12}$$

where R_u is the universal gas constant and W is the mean molecular weight of the mixture, which is defined as:

$$\frac{1}{W} = \sum_{k=1}^{N}\frac{Y_k}{W_k} \tag{A.13}$$

Conservation of species

A reacting flow fluid consist of many different species. During the non-premixed combustion process, numerous molecules are created and destroyed due to chemical reactions and mixing of the different species in the fluid occurs. The behaviour of each species in such a fluid flow can be described by its own conservation equation, which reads:

$$\frac{\partial \rho Y_k}{\partial t} + \frac{\partial}{\partial x_i}\left(\rho u_{k,i} Y_k\right) = \rho\dot{\omega}_k \tag{A.14}$$

where $u_{k,i}$ is the velocity of species k in direction i and $\dot{\omega}_k$ is the source term for species k. Because of conservation of particles, the summation of the source terms equal zero:

$$\sum_{k=1}^{N}\dot{\omega}_k = 0 \tag{A.15}$$

When looking at Eq.(A.14), it can be seen that the viscous term depends on the velocity of species k. This needs to be rewritten in terms of the velocity of the fluid u_i. To reach this goal, the velocity of species k is rewritten as follows:

$$u_{k,i} = u_i + V_{k,i} \tag{A.16}$$

where $V_{k,i}$ is the diffusion velocity and denotes the difference between the velocity of species k and the velocity of the fluid. By definition, the following statement holds for the diffusion velocity:

$$\sum_{k=1}^{N} Y_k V_{k,i} = 0 \tag{A.17}$$

Combining Eq.(A.14) with the definition of the diffusion velocity Eq.(A.16) and the continuity equation Eq.(A.6), the result is:

$$\rho \frac{\partial Y_k}{\partial t} + \rho u_i \frac{\partial Y_k}{\partial x_i} = \rho \frac{DY_k}{Dt} = -\frac{\partial}{\partial x_i}\left(\rho V_{k,i} Y_k\right) + \rho \dot{\omega}_k \tag{A.18}$$

Next step is to find the diffusion velocities $V_{k,i}$ for N species which are present in the fluid flow. In the work of Williams [53], it is stated that the diffusion velocity can be obtained by solving the following system:

$$\begin{aligned} \frac{\partial X_m}{\partial x_i} = &\sum_{k=1}^{N} \frac{X_m X_k}{D_{mk}} \left(V_{k,i} - V_{m,i}\right) + \left(Y_m - X_m\right)\left(\frac{1}{p}\frac{\partial p}{\partial x_i}\right) \\ &+ \frac{\rho}{p}\sum_{k=1}^{N} Y_m Y_k \left(f_{m,i} - f_{k,i}\right) + \sum_{k=1}^{N}\left(\frac{X_k X_m}{\rho D_{mk}}\right)\left(\frac{\alpha_k}{Y_k} - \frac{\alpha_m}{Y_m}\right)\left(\frac{1}{T}\frac{\partial T}{\partial x_i}\right) \end{aligned} \tag{A.19}$$

where D_{mk} is the binary mass diffusion coefficient of species m into species k and α_k is the thermal diffusivity of species k. The last term is also known as the Soret effect and indicates the diffusion of mass due to temperature gradients. The presented system is linear and the size is N^2 and has to be solved in each direction, for every time step and grid point. Due to the complexity of the considered system, solving this is a complicated and computational costly exercise[12]. Therefore in most codes, simplifications are used and the Soret effect is neglected. The first simplification is to consider binary diffusion.

In binary diffusion, the mixture consists of only two species, species A and species B. If pressure gradients are small and body forces are neglected, Eq.(A.19) reduces to its simplified form, which is given by:

$$\frac{\partial X}{\partial x_i} = \frac{X_A X_B}{D_{AB}}\left(V_{B,i} - V_{A,i}\right) \tag{A.20}$$

When considering that the summation over all mass fractions equals one and Eq.(A.17), Eq (A.20) can be rewritten as:

$$-V_A Y_{A,i} = D_{AB}\frac{\partial Y_A}{\partial x_i} \tag{A.21}$$

where D_{AB} is the binary diffusion coefficient. The expression above is known as Fick's law and is exact for diffusion of two species. However, when a multi species mixture is considered, Eq.(A.21) does not hold and a more complex expression must be used or simplifications have to be implemented.

Let's consider a fluid with N species, which means that multicomponent diffusion of the N components has to be considered. One species is selected as carrier gas. This gas is abundant in the mixture. For example, nitrogen is considered as carrier gas when a mixture with air is considered. In the presentation of the simplifications for multicomponent diffusion, the carrier gas has index $k = N$. When considering Fick's law, the multicomponent version reads:

$$-(V_{k,i}Y_k)_{\text{Fick}} = D_{kN}\frac{\partial Y_k}{\partial x_i} \quad \text{for } k = 1...N-1 \tag{A.22}$$

D_{kN} is the binary diffusion coefficient of species k and the carrier gas with index N. This means that the mass diffusion species k depends on the properties of species k and species N.

Another method to model multicomponent diffusion is Wilke's law, where also one fluid is selected as carrier gas. However, the mass diffusion of species k is related to the properties of species k and properties of the mixture itself. Wilke's law reads:

$$-(V_{k,i}Y_k)_{\text{Wilke}} = D_{km}\frac{\partial Y_k}{\partial x_i} \quad \text{for } k = 1...N-1 \tag{A.23}$$

where D_{km} is the composition dependent diffusion coefficient of species k in the mixture.

The approximation introduced by Fick's law is a good approximation for turbulent diffusion flames necessary for turbulent non-premixed combustion. In such a flame, turbulent transport has a significant contribution compared to molecular transport [36].

Conservation of energy

The conservation of energy equations requires special care because of the existence of multiple forms. For example, the energy or enthalpy formulation can be considered. In the list below, several options are presented including the reason to use this specific form:

- Specific energy: suitable for liquids
- Specific total energy: suitable in studies where compressibility effects are important (acoustics)
- Specific enthalpy: suitable in studies of combustion at almost constant pressure
- Temperature: to see the reasons for temperature change

In this thesis, acoustics are not considered. Therefore the enthalpy formulation is used and presented in this subsection. Enthalpy exists of sensible enthalpy, which is dependent on temperature,

and chemical enthalpy:

$$h_k = \int_{T_0}^{T} C_{p,k}(T)dT + \Delta h^0_{f,k} = h_{s,k} + \Delta h^0_{f,k} \tag{A.24}$$

where h_k is the enthalpy of species k per unit mass, or specific enthalpy. $C_{p,k}$ is the specific heat at constant pressure for species k, $\Delta h^0_{f,k}$ is the enthalpy of formation for species k and $h_{s,k}$ is the specific sensible enthalpy for species k. The specific enthalpy of the mixture is defined as the mass-weighted sum over the specific enthalpies h_k:

$$\begin{aligned} h &= \sum_{k=1}^{N} h_k Y_k = \sum_{k=1}^{N} Y_k \left(\int_{T_0}^{T} C_{p,k}(T)dT + \Delta h^0_{f,k} \right) \\ &= \int_{T_0}^{T} C_p(T)dT + \Delta h^0_f = h_s + \Delta h^0_f \end{aligned} \tag{A.25}$$

The conservation equation of specific enthalpy is written as:

$$\frac{\partial \rho h}{\partial t} + \frac{\partial}{\partial x_i}\left(\rho u_i h\right) = -\frac{\partial q_i}{\partial x_i} + \tau_{ij}\frac{\partial u_i}{\partial x_j} + \dot{Q} + \frac{Dp}{Dt} + \rho \sum_{k=1}^{N} Y_k f_{k,j} V_{k,j} \tag{A.26}$$

where $\dot{Q}$ is the heat source term (e.g. radiation, sparks, lasers), $\rho \sum_{k=1}^{N} Y_k f_{k,j} V_{k,j}$ is the power produced by volume force f_k on species k, q is the diffusive energy flux and $\Phi_{visc} = \tau_{ij}\frac{\partial u_i}{\partial x_j}$ is the viscous dissipation function. When combining Eq.(A.26) with Eq.(A.6), the result is:

$$\rho\frac{\partial h}{\partial t} + \rho u_i \frac{\partial h}{\partial x_i} = \rho\frac{Dh}{Dt} = -\frac{\partial q_i}{\partial x_i} + \Phi_{visc} + \dot{Q} + \frac{Dp}{Dt} + \rho \sum_{k=1}^{N} Y_k f_{k,j} V_{k,j} \tag{A.27}$$

The diffusive energy flux consists of conduction, the energy flux related to the diffusion of species with different enthalpy (inter-diffusion) and the energy flux due to mass concentration gradients. This is also known as the Dufour Effect and it's the reciprocal phenomenon to the of Soret effect. Thus, the diffusive energy flux becomes:

$$\begin{aligned} q_i &= q_{i,\text{conduction}} + q_{i,\text{inter-diffusion}} + q_{i,\text{Dufour}} \\ &= -\kappa\frac{\partial T}{\partial x_i} + \rho \sum_{k=1}^{N} h_k Y_k V_{k,i} + R_u T \sum_{k=1}^{N}\sum_{m=1}^{N} \left(\frac{X_m \alpha_m}{W_k D_{km}}\right)(V_{k,i} - V_{m,i}) \end{aligned} \tag{A.28}$$

where κ is the thermal conductivity of the mixture and T is the temperature of the mixture.

With the presented continuity equation,conservation of momentum, species and energy equations, $N + 5$ equations are presented needed to solve the system of equations related to compressible, laminar reacting flow. However when considering non-premixed combustion, in most cases it is useful to use simplifications in order to reduce computational costs and to reduce the complexity of the problem. In Subsection A.1.3, these simplifications are further elaborated.

Relevant dimensionless numbers

Dimensionless numbers in a engineering or scientific problem are a set of dimensionless quantities which describe the system and can give an order-of-magnitude estimate about the behaviour of

the system. Often such a dimensionless number is defined by the ration of two physical quantities. In this subsection the relevant dimensionless numbers are found for reacting flow.

The Reynolds number is defined as the ratio of inertial forces to viscous forces and therefore quantifies the relative importance of these two types of forces for given flow conditions. It's given by:

$$Re = \frac{\rho u L}{\mu} = \frac{u L}{\nu} \tag{A.29}$$

where ν is the kinematic viscosity coefficient. In general, it can be stated that a low Reynolds number corresponds to laminar flow and a high Reynolds number (in the order of 10.000) is related to turbulent flow.

The Lewis number characterizes fluid flows where mass diffusion and heat transfer are present in the flow and it is defined as the ratio of thermal diffusion to mass diffusion of species k:

$$Le_k = \frac{\kappa}{\rho C_p D_k} = \frac{D_{th}}{D_k} \tag{A.30}$$

The Prandtl number is defined as the ratio of momentum diffusivity to the thermal diffusivity and it's given by:

$$Pr = \frac{\nu}{\kappa/(\rho C_p)} = \frac{\mu C_p}{\kappa} \tag{A.31}$$

The Schmidt number characterizes fluid flows with momentum diffusivity and mass diffusivity of species k, for example a fluid flow of a mixture. The Schmidt number is defined as:

$$Sc = \frac{\nu}{D_k} = Le_k \cdot Pr \tag{A.32}$$

The definition of the Damköhler number depends on the combustion mechanism, usually it's defined as the ratio of a flow time scale and a chemical time scale. The Damköhler number characterizes the combustion regime of a particular type of combustion mechanism. For non-premixed combustion, the Damköhler number is defined as the ratio of time scale for mixing and time scale for chemical reactions:

$$Da = \frac{\tau_{mix}}{\tau_c} \tag{A.33}$$

where τ_c is the chemical time scale and τ_{mix} is the time scale for mixing.

A.1.2 Chemical kinetics

Chemistry plays an important role in combustion. Exothermic chemical reactions produces heat when one species is converted into another species. The released heat can be used for other

purposes, such as generating power. The creation or destruction of species is described by its instantaneous source term $\dot{\omega}_k$. It is possible to compute this term by using the properties of the elementary chemical reactions.

Chemical reaction describes the conversion of species before and after a reaction. When describing the chemical reaction of a simple combustible gas, a large number of elementary chemical reactions takes place which also describe the creation and destruction of intermediate species. For example, the detailed reaction scheme for combustion of natural gas contains 325 reactions and 53 species, which is known as the GRI-MECH 3.0 mechanism [49]. This optimized mechanism describes basic combustion properties and basic chemical kinetics.

A chemical reaction can be described as:

$$\sum_{k=1}^{N_s} \nu'_{kj} M_k \rightarrow \sum_{k=1}^{N_s} \nu''_k M_k \text{ for } \quad j = 1..N_r \tag{A.34}$$

where M_k is a symbol for species k, ν'_{kj} and ν''_{kj} are the stoichiometric coefficients for species k in reaction j of the reactants and products respectively and N_s is the number of species. The stoichiometric coefficients describe the number of species needed to have an optimal chemical reaction.

Due to mass conservation in a chemical reaction, the following holds:

$$\sum_{k=1}^{N_r} \nu_{kj} W_k = 0 \tag{A.35}$$

where $\nu = \nu''_{kj} - \nu'_{kj}$. Now the reaction rate $\dot{\omega}_k$ of species k can be determined by using:

$$\dot{\omega}_k = \sum_{j=1}^{N_r} \omega_{kj} = W_k \sum_{j=1}^{N_r} \nu_{kj} \mathcal{Q}_j \tag{A.36}$$

where $\mathcal{Q}_j$ is the rate of progress of reaction j. $\mathcal{Q}_j$ is also written as:

$$\mathcal{Q}_j = k_{fj} \prod_{k=1}^{N_s} [X_k]^{\nu'_{kj}} - k_{rj} \prod_{k=1}^{N_s} [X_k]^{\nu''_{kj}} \tag{A.37}$$

where k_{rj} and k_{fj} are the reversed and forward rates of reaction j respectively, $[X_k]$ is the concentration of species k where the superscript denotes the concentration of species of reactants (ν'_{kj}) or products (ν''_{kj}). The non-linearity of source terms is due to the rate constants k_{fj} and k_{rj}, where k_{fj} is modelled using the empirical Arrhenius law:

$$k_{fj} = B_{fj} T^{\alpha_j} \exp\left(-\frac{E_{aj}}{R_u T}\right) = B_{fj} T^{\alpha_j} \exp\left(-\frac{T_{a_j}}{T}\right) \tag{A.38}$$

where B_{fj} is the pre-exponential constant, α_j is the temperature exponent in reaction j , T_{aj} is the activation temperature and $E_{aj} = R_u T_{aj}$ is the activation energy.

When looking at the non-linear behaviour of the reaction rate and the number of elementary chemical reactions in a detailed chemical reaction mechanism, it is shown that chemistry in combustion is a major issue. The computational costs of describing combustion with such a detailed scheme as GRI-MECH 3.0 are enormous. Especially in turbulent combustion, where temperature and species mass fraction are fluctuating, the computational time increases dramatically. Therefore in most numerical approaches, the important combustion properties are selected and the corresponding species are identified and others are discarded in order to limit the number of species and the number of elementary chemical reactions. Such reduction of a chemical scheme can be done by hand or automatically. For example, the global schemes can be calculated by hand. It relies on two assumptions [41], namely quasi-steady state approximation and partial equilibrium. But identifying limiting steps, quasi-steady state species and equilibrium reaction in a complex detailed chemical system is a very difficult task. Also, due to the reduction, the reaction rates are described by complicated , stiff expressions. Because of these difficulties, the description of chemistry in combustion nowadays can be categorized into two groups: automatic chemistry reduction or tabulated chemistry [42].

A.1.3 General aspects of laminar non-premixed flames

Non-premixed combustion is characterized by the presence of a non-premixed (or diffusion) flame. In such a flame, fuel and oxidizer are present in a separate stream. Fuel and oxidizer come together and mixes due to molecular diffusion in a thin layer such that a combustible mixture is created. If ignition occurs, the combustible mixture ignites and heat is released. Far away from the reaction layer, the mixture is either too lean or too rich (see Fig. 2.1).

The common methodology of solving non-premixed combustion problem is to decompose this problem in two sub-problems, namely:

1. A mixing problem, in which the output are flow and mixture variables;

2. A flame structure problem, in which the output of the mixing problems are used to determine the chemistry information

The derivation of the mixing problem starts with the governing equations presented in Section A.1. The starting point was a compressible fluid flow which consists of multiple species. However for most practical cases in which non-premixed combustion occurs, the low-Mach number assumption is imposed [53, 36]. This is a reasonable assumption if acoustic waves are not taken into account and the flame propagation speed of the flame front in the fluid flow is low compared to the speed of sound. The former is also known as the deflagration regime and this is typical for non-premixed combustion. When the low-Mach number assumption is imposed, compressibility effects, viscous heating and the $\frac{Dp}{Dt}$ in Eq.(A.27) can be neglected and density is independent of the pressure, but may change due to temperature difference and mixing of species with different density [41]. Also it is common to use a transport equation for temperature when the low-Mach number approximation is used. This equation can be obtained by taking the derivative of Eq.(A.25) and omitting the

$\Delta h^0_{f,k}$ term, the following expression can be obtained [41].

$$\rho C_p \frac{DT}{Dt} = \dot{\omega}_T + \frac{\partial}{\partial x_i}\left(\kappa \frac{\partial T}{\partial x_i}\right) - \rho \frac{\partial T}{\partial x_i}\left(\sum_{k=1}^{N} C_{p,k} Y_k V_{k,i}\right) + \dot{Q} + \rho \sum_{k=1}^{N} Y_k f_{k,i} V_{k,i} \tag{A.39}$$

where $\dot{\omega}_T$ is the heat released due to combustion and it is defined as:

$$\dot{\omega}_T = -\sum_{k=1}^{N} h_k \dot{\Omega}_k = -\sum_{k=1}^{N} h_{s,k} \dot{\omega}_k - \sum_{k=1}^{N} \Delta h^0_{f,k} \dot{\omega}_k \tag{A.40}$$

When assuming low-Mach number flow, therefore neglecting viscous heating, and simplifying the temperature equation by assuming equal specific heat capacities $C_{p,k}$ for all species and assuming a constant pressure flame, the result is:

$$\rho C_p \frac{DT}{Dt} = \dot{\omega}_T + \frac{\partial}{\partial x_i}\left(\kappa \frac{\partial T}{\partial x_i}\right) + \dot{Q} + \rho \sum_{k=1}^{N} Y_k f_{k,i} V_{k,i} \tag{A.41}$$

The assumption on equal specific heat capacities for all species is not often true, but it is often used in non-premixed combustion calculations [41]. In summary, the transport equation for temperature is a simplified version of the energy transport equation and it is mainly used for the study of non-premixed combustion and its modelling.

In many non-premixed combustion studies an idealized situation is assumed in which the chemical reaction is irreversible and infinitely fast, which means that reaction is finished and found an equilibrium before the flow changed locally the composition of the mixture. When this idealized situation is treated, the mass fractions of all species and the temperature is a function of a passive scalar, which is known as the mixture fraction. The derivation of the transport equation of the mixture fraction starts with the transport equation of species for the fuel and oxidizer and by modelling diffusion with Fick's law with equal diffusion coefficient $D_{kN} = D$ for all species and neglecting the body forces. Eq.(A.14) then becomes:

$$\frac{\partial \rho Y_F}{\partial t} + \frac{\partial}{\partial x_i}\left(\rho u_i Y_F\right) = \frac{\partial}{\partial x_i}\left(\rho D_F \frac{\partial Y_F}{\partial x_i}\right) + \rho \dot{\omega}_F \tag{A.42}$$

$$\frac{\partial \rho Y_O}{\partial t} + \frac{\partial}{\partial x_i}\left(\rho u_i Y_O\right) = \frac{\partial}{\partial x_i}\left(\rho D_O \frac{\partial Y_O}{\partial x_i}\right) + \rho s \dot{\omega}_F \tag{A.43}$$

where the following relation for the reaction term of the oxidizer is used:

$$\dot{\omega}_O = s \dot{\omega}_F \tag{A.44}$$

where s is the mass stoichiometric ratio, defined as $s = \frac{\nu_O W_O}{\nu_F W_F}$.

The derivation of the relation between temperature and mixture fraction starts with Eq.(A.41), neglecting $\dot{Q}$ and body forces and by using the following relation between the reaction term of the fuel and the heat release due to combustion:

$$\dot{\omega}_T = -Q \dot{\omega}_F \tag{A.45}$$

where Q is heat of reaction per unit mass. Now Eq.(A.41) becomes:

$$\rho\frac{\partial T}{\partial t}+\rho u_i\frac{\partial T}{\partial x_i}=-\frac{Q}{C_p}\dot{\omega}_F+\frac{\partial}{\partial x_i}\left(\frac{\kappa}{C_p}\frac{\partial T}{\partial x_i}\right) \tag{A.46}$$

Combining Eq.(A.42), (A.43) (A.46) and assuming a Lewis number of 1 for all species, it can be shown the the following three quantities:

$$z_1=sY_F-Y_O \tag{A.47a}$$

$$z_2=\frac{C_pT}{Q}+Y_F \tag{A.47b}$$

$$z_3=\frac{sC_pT}{Q}+Y_O \tag{A.47c}$$

have the transport equation, namely:

$$\frac{\partial\rho z}{\partial t}+\frac{\partial}{\partial x_i}\left(\rho u_i z\right)=\frac{\partial}{\partial x_i}\left(\rho D_z\frac{\partial z}{\partial x_i}\right) \tag{A.48}$$

The three quantities follow the presented transport equation Eq.(A.48), but have different boundary conditions on the fuel side and the oxidizer side. When the quantities are normalized by the following definition:

$$Z=\frac{z_j-zj^O}{z_j^F-z_j^O} \tag{A.49}$$

The result is that all normalized variables follow the same transport equation and have the same boundary conditions. The transport equation becomes:

$$\frac{\partial\rho Z}{\partial t}+\frac{\partial}{\partial x_i}\left(\rho u_i Z\right)=\frac{\partial}{\partial x_i}\left(\rho D_Z\frac{\partial Z}{\partial x_i}\right) \tag{A.50}$$

where Z is the mixture fraction with boundary condition $Z=1$ in the fuel stream and $Z=0$ in the oxidizer stream(see Fig. 2.2). With the introduction of the mixture fraction Z the number of variables is reduced with $N-1$. It is also noted that the mixture fraction is a passive scalar, due to the absence of a reaction term in the transport equation. The latter is a direct result of the infinitely fast chemistry assumption.

For some application, enthalpy is used as a passive scalar which also follows transport Eq.(A.50). This can be shown by imposing the same assumptions as with the derivation of the transport equation of temperature as mixture fraction. When these assumptions are imposed and combining Eq.(A.27) and Eq.(A.28) the result is the following expression:

$$\frac{\partial\rho h}{\partial t}+\frac{\partial}{\partial x_i}\left(\rho u_i h\right)=-\frac{\partial}{\partial x_i}\left(-\kappa\frac{\partial T}{\partial x_j}+\rho\sum_{k=1}^{N}h_kY_kV_{k,j}\right) \tag{A.51}$$

When assuming a Lewis number of 1, using Eq.(A.22) for the diffusion velocity and using $\frac{\partial h_k}{\partial x_i}=C_{p,k}\frac{\partial T}{\partial x_i}$, the result after some manipulations is:

$$\frac{\partial\rho h}{\partial t}+\frac{\partial}{\partial x_i}\left(\rho u_i h\right)=\frac{\partial}{\partial x_i}\left(D_{th}\frac{\partial h}{\partial x_i}\right) \tag{A.52}$$

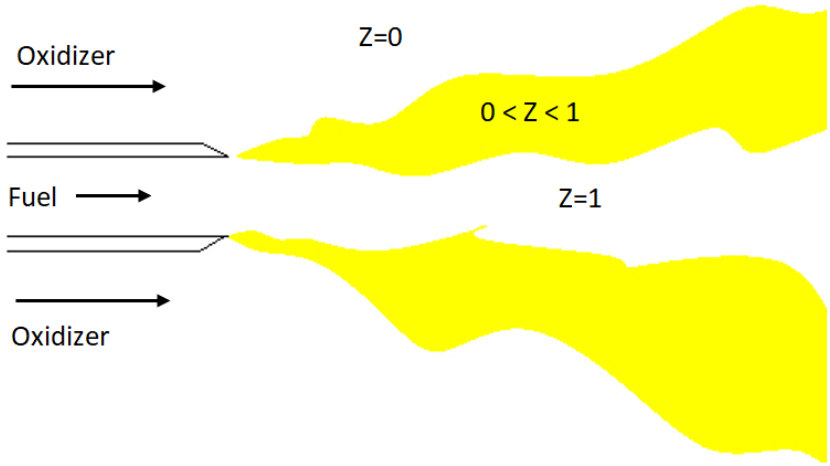

Figure A.1: Representation of the mixture fraction in a jet flow

With the determination of the mixture fraction, all aspects of the mixing problem has been solved.

Next step in a non-premixed combustion problem is solving the flame structure problem. In the flame structure problem the chemical characteristics are solved. The determination of the flame structure problem starts with a variable change transformation. The coordinate transformation is applied on the mass fraction equations for all species and temperature equation and the transformation from (x_1, x_2, x_3, t) to (z, y_2, y_3, t) where y_2 and y_3 are spatial variables in planes which are parallel to iso-Z surfaces. See Fig. A.2 for a 2D representation of the proposed coordinate transformation.

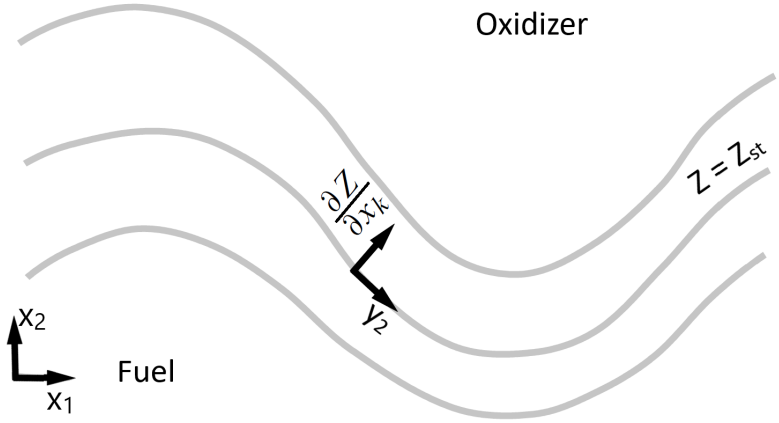

Figure A.2: 2D representation of the coordinate transformation for diffusion flames. The y_3 direction is normal to the $\frac{\partial Z}{\partial x_k}$-$y_2$ plane

When the presented coordinate transformation has been performed , the resulting equations contain terms which corresponds to the gradients along the flame front (thus, along y_2 and y_3) and to gradients normal to the flame front. In the specific case that a flame front is very thin compared

to other flow and wrinkling scales, the gradients along the flame front can be neglected comparing to the gradient normal to the flame front. This implies that the flame structure is locally 1D and depends on time and mixture fraction. Such a small element of the flame front which shows 1D behaviour is called a flamelet and therefore this assumption is called the flamelet assumption.

When this assumption is applied, the species mass equation can be written as:

$$\rho\frac{\partial Y_k}{\partial t}+\frac{\partial Y_k}{\partial Z}\left[\rho\frac{\partial Z}{\partial t}+\rho u_i\frac{\partial Z}{\partial x_i}-\frac{\partial}{\partial x_i}\left(\rho D\frac{\partial Z}{\partial x_i}\right)\right]-\rho D\left(\frac{\partial Z}{\partial x_i}\frac{\partial Z}{\partial x_i}\right)\frac{\partial^2 Y_k}{\partial Z^2}=\rho\dot{\omega}_k \tag{A.53}$$

The term within the brackets of Eq.(A.53) disappears because of Eq.(A.50). The result becomes:

$$\rho\frac{\partial Y_k}{\partial t}=\rho\dot{\omega}_k+-\rho D\left(\frac{\partial Z}{\partial x_i}\frac{\partial Z}{\partial x_i}\right)\frac{\partial^2 Y_k}{\partial Z^2}=\rho\dot{\omega}_k+\frac{1}{2}\rho\chi\frac{\partial^2 Y_k}{\partial Z^2} \tag{A.54}$$

where the term in the parenthesis is called the scalar dissipation rate χ and is a measure of mixing in the fluid flow:

$$\chi=2D_k\left(\frac{\partial Z}{\partial x_i}\frac{\partial Z}{\partial x_i}\right) \tag{A.55}$$

The temperature equation can also be rewritten in such a form:

$$\rho\frac{\partial T}{\partial t}=\dot{\omega}_T+\frac{1}{2}\rho\chi\frac{\partial^2 T}{\partial Z^2} \tag{A.56}$$

It can be concluded that temperature T and mass fraction Y_k can be written as function of time and mixture fraction. Eq.(A.54) and (A.56) are the flamelet equation which describes the flame structure. This approach is widely used in non-premixed combustion calculations. When looking at these equations, it can be seen that only the scalar dissipation rate χ is dependent on spatial variables x_i. This means that once χ is specified, the flamelet equations can be solved in Z-space and therefore the necessary thermochemical variables can be determined.The application of the flamelet equations based on the mixture fraction has its origin in the papers of Peters [37] and Kuznetsov [31].

In summary, to rewrite the governing equations for compressible, reacting flow to the presented flamelet equations, the following assumptions have been applied:

1. Acoustic interaction and viscous dissipation neglected
2. Almost constant pressure flame
3. Low Mach number approximation
4. Radiative heat loss neglected

5. External forces neglected
6. Ideal gas mixture
7. All molecules have the same molecular diffusion coefficient $D_{kN} = D$
8. Heat and species diffuse in the same way, therefore the Lewis number is equal to unity $Le_k = Le = \frac{\lambda}{\rho c_p D} = 1$
9. Soret (molecular diffusion due to temperature gradients) and Dufour (heat flux due to species mass fraction gradients) effects neglected.
10. Same diffusion coefficient for all species
11. Infinitely, fast chemistry
12. Flamelet assumption

Flamelet/progress variable approach

Imposing the assumption of irreversible, infinitely fast chemistry to solve the flame structure problem leads to a description of the problem which is only dependent of the mixture fraction Z and therefore contains no information about chemical reactions and cannot account for chemical variations in directions perpendicular to its gradient [39]. The results of imposing the mentioned assumption is that flame lift-off and other ignition and extinction phenomena cannot be predicted accurately [40]. One solution for this problem is to apply the flamelet/progress variable approach, developed by Pierce and Moin [39]. The idea of the approach is to introduce another tracking scalar which is independent of the mixture fraction. This means that the new scalar must be a non-conserved scalar, in this case the reaction progress variable ϕ. The concept of a progress variable is borrowed from the description of chemistry for premixed and partially-premixed combustion and it measures the extent-of-reaction of the flow. For example, the progress variable could be defined as a normalized summation of the mass fractions of reaction products. By definition, the progress variable is equal to 0 in fresh gasses and 1 in fully-burnt gasses. The corresponding transport equation is:

$$\frac{\partial \rho\phi}{\partial t} + \frac{\partial}{\partial x_i}\left(\rho u_i \phi\right) = \frac{\partial}{\partial x_i}\left(\rho D_\phi \frac{\partial \phi}{\partial x_i}\right) + \rho\dot{\omega}_\phi \tag{A.57}$$

The application of the flamelet/progress variable approach results in a flame structure problem in which thermochemical variables are dependent on Z and ϕ, such as:

$$Y_k = Y_k(Z,\phi) \tag{A.58a}$$
$$T = T(Z,\phi) \tag{A.58b}$$
$$\dot{\omega}_\phi = \dot{\omega}_\phi(Z,\phi) \tag{A.58c}$$

The methodology to solve the presented flame structure problem is given in Paragraph **??**.

A.2 Turbulent non-premixed combustion

Turbulent flow is characterized by the presence of eddies and the vortices which are stretched and twisted by the velocity field under the influence of the vorticity distribution. Therefore the induced velocity field interacts with the vortices and also influences the evolution of the vortices. A turbulent velocity field shows a broad spectrum of eddy sizes, however dissipation of the flow only occurs at the smallest eddies. This behaviour is also known as the energy cascade, and it describes the transfer of energy from the largest eddies to the smallest structures until it is finally dissipated on molecular scales. The idea behind this concept is that the largest eddies, which are created by instabilities in the mean flow, are exposed to inertial instabilities. This results in a break-up into smaller eddies. Also the smaller eddies are subjected to instabilities, which leads to break-up of the smaller eddies. This mechanism repeats itself, until the smallest structures are reached and then finally the smallest eddies will dissipate its energy.

Therefore, the presence of turbulence in a reacting flow causes that chemical reactions and mixing could be altered due to the properties of turbulence. The effect of turbulence on combustion and vise versa is presented in next the subsection. The third and fourth subsection deals with the turbulent version of respectively the mixing problem and the flame structure problem. Last subsection shows an implementation of the presented turbulent non-premixed models in an attempt to mimic the behaviour of the Delft-Jet-in-Hot-Coflow flame.

A.2.1 Effect of turbulence on combustion and combustion on turbulence

As presented in Section 1.1, there is a two-way coupling between chemistry and turbulence. In summary, the heat of the flame causes strong flow accelerations in the turbulent flow and causes a change in kinematic viscosity due to the temperature change. Vise versa, turbulence improves mixing, which enhances chemical reactions. An elaboration of the presented interaction is illustrated in Figure A.3. Because combustion requires that fuel and oxidizer be mixed at the molecular level, the turbulent mixing process is important in non-premixed combustion in turbulent flow. Such a flow exists of a spectrum of different eddy-scales.The large eddies are responsible for entrainment of the reactants. This effect is also known as large-scale macro mixing. The widely accepted view is that once a range of different size eddies has developed, strain and shear at the interface between eddies improves the mixing of the flow. During the break-up of larger eddies into smaller eddies, strain and shear increases and this will steepen the concentration gradients at the interface between reactants. This causes an enhancement of their molecular inter-diffusion [36]. When chemical reaction occur in the thin reaction layer, heat and reactants are released. The formed causes volume expansion and therefore an increase in shear and pressure, which also alters the turbulent flow. Also some chemical properties, such as viscosity and specific heat at constant pressure are dependent on temperature. These temperature-dependent chemical properties changes due to the release of heat and this will alter the turbulent flow as well.

But turbulent flow can also affect combustion in a negative way. As stated previously, chemistry occurs in a very thin layer, the flame front. If the flame front is thin compared to the Kolmogorov length scale, which is the smallest scale in a turbulent flow, the flamelet assumption can be

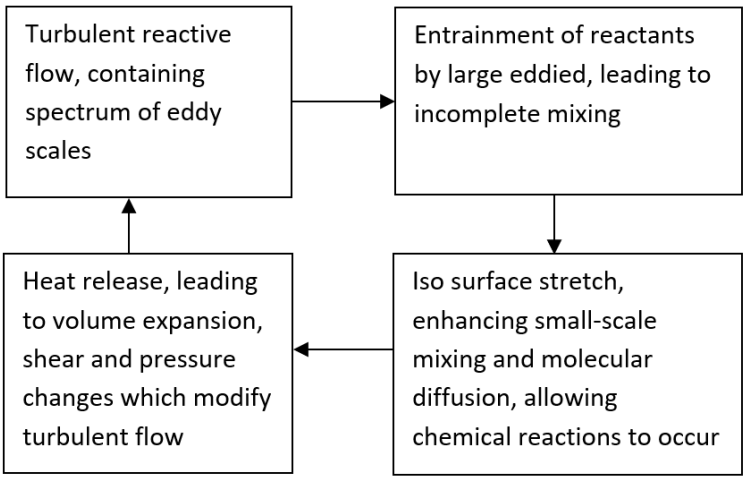

Figure A.3: Interaction between turbulent flow and chemistry [3]

applied. However, when turbulence is so intense that the Kolmogorov length scale is smaller than the flame front,the smallest eddies can penetrate the flame front and destroy its structure. This could result in an extinguished flame [36].

Appendix B

Detailed coarse mesh SMP results

B.1 Detailed τ results

Table B.1: Error of $\langle\phi\rangle$ with respect to the reference case for several fine-scale models and selected τ_ϕ

Fine-scale model	τ_u	τ_ϕ	Number of elements		
			300	200	100
VMM leading subscales	Adj. Sh.	Cod.	1.489×10^{-3}	3.778×10^{-3}	7.482×10^{-3}
VMM leading subscales	Adj. Sh.	F&V	1.544×10^{-3}	3.820×10^{-3}	7.504×10^{-3}
VMM leading subscales	Adj. Sh.	Sh.	1.506×10^{-3}	3.770×10^{-3}	7.402×10^{-3}
VMM leading subscales	Adj. Sh.	Adj. Sh.	1.509×10^{-3}	3.773×10^{-3}	7.403×10^{-3}
VMM leading subscales	Sh.	Cod.	1.627×10^{-3}	3.879×10^{-3}	7.420×10^{-3}
VMM leading subscales	Sh.	F&V	1.684×10^{-3}	3.934×10^{-3}	7.450×10^{-3}
VMM leading subscales	Sh.	Sh.	1.649×10^{-3}	3.881×10^{-3}	7.341×10^{-3}
VMM leading subscales	Sh.	Adj. Sh.	1.652×10^{-3}	3.884×10^{-3}	7.342×10^{-3}

Table B.2: Error of $\langle Z \rangle$ with respect to the reference case for several fine-scale models and selected τ_Z

Fine-scale model	τ_u	τ_Z	Number of elements		
			300	200	100
VMM leading subscales	Adj. Sh.	Cod.	2.211×10^{-3}	6.058×10^{-3}	9.421×10^{-3}
VMM leading subscales	Adj. Sh.	F&V	2.324×10^{-3}	6.142×10^{-3}	9.468×10^{-3}
VMM leading subscales	Adj. Sh.	Sh.	2.274×10^{-3}	6.057×10^{-3}	9.313×10^{-3}
VMM leading subscales	Adj. Sh.	Adj. Sh.	2.280×10^{-3}	6.062×10^{-3}	9.314×10^{-3}
VMM leading subscales	Adj. Sh.	st. des.	2.188×10^{-3}	5.983×10^{-3}	9.284×10^{-3}
VMM leading subscales	Sh.	Cod.	2.410×10^{-3}	6.173×10^{-3}	9.357×10^{-3}
VMM leading subscales	Sh.	F&V	2.526×10^{-3}	6.273×10^{-3}	9.417×10^{-3}
VMM leading subscales	Sh.	Sh.	2.477×10^{-3}	6.186×10^{-3}	9.254×10^{-3}
VMM leading subscales	Sh.	Adj. Sh.	2.483×10^{-3}	6.191×10^{-3}	9.256×10^{-3}
VMM leading subscales	Sh.	st. des.	2.394×10^{-3}	6.104×10^{-3}	9.222×10^{-3}